establishing *Aire*$^{+/gfp\text{-}neo}$ mice, they were crossed with a general deleter Cre recombinase-expressing transgenic line (21) to remove the neo^r gene cassette, which contains the herpes simplex virus *thymidine kinase* gene promoter for efficient neo^r gene expression. After confirming the removal of the neo^r gene cassette (Fig. 1 B), mice were crossed with C57BL/6 mice to select a line containing the GFP knock-in allele but not the Cre recombinase-expressing transgenic allele. *Aire*$^{+/gfp}$ mice were then crossed to obtain *Aire*$^{gfp/gfp}$ mice, which have a null mutation for the *Aire* gene because of disruption of the *Aire* gene by insertion of the GFP gene (Fig. 1 B). As expected, *Aire*$^{gfp/gfp}$ mice, but not *Aire*$^{+/gfp}$ mice, showed no expression of endogenous Aire in the thymus, as detected with polyclonal anti-Aire antibody (Ab) recognizing peptides located within the proline-rich region of Aire (unpublished data).

Using immunohistochemistry, we first examined whether GFP expression from *Aire*$^{+/gfp}$ mouse thymus reflects endogenous *Aire* gene expression. Stromal cells showing variable extents of GFP expression in the cytoplasm and nucleus were scattered throughout the thymic medulla (Fig. 1 C). The medullary region was identified by staining with *Ulex europaeus* agglutinin 1 (UEA-1) (Fig. 2 A), anti–epithelial cell adhesion molecule 1 (EpCAM) mAb (Fig. 2 B), or anti–keratin 5 (K5) Ab (Fig. S1 A, available at http://www.jem.org/cgi/content/full/jem.20080046/DC1). GFP-expressing cells from *Aire*$^{+/gfp}$ mouse thymus showed a dendritic to fibroblastic morphology and were enriched at the cortico-medullary junction (Fig. 1 C; Fig. 2, A and B; and Fig. S1 A). When doubly stained with anti-Aire Ab, most of the GFP-expressing cells contained variable amounts of Aire nuclear dots within their nuclei (Fig. 1 C), indicating that GFP expression is under the transcriptional control of the authentic *Aire* gene. However, a few cells showed Aire nuclear dots without any detectable GFP expression (Fig. 1 C, arrows) or expressed GFP without obvious Aire nuclear dots (not depicted). As expected, *Aire*$^{+/+}$ mouse thymus showed no GFP signals (Fig. 2, A and B). Notably, most of the CD11c-positive DCs in the thymus were GFP negative (Fig. S1 B), suggesting that Aire expression from thymic DCs is negligible compared with that from mTECs.

Altered thymic organization in Aire-deficient mice

We then examined the effect of Aire deficiency on thymic organization in *Aire*$^{gfp/gfp}$ mouse thymus sections, focusing on the production of cells genetically marked with GFP and, therefore, active in *Aire* gene transcription but lacking functional Aire protein. There were many GFP$^+$ "Aire-less" TECs within the medulla (Figs. 2, A and B; and Fig. S1 A), indicating clearly that Aire protein itself is not necessary for the production of particular mTEC lineages committed to express Aire. However, detailed inspection demonstrated that the morphology and location of GFP$^+$ cells from *Aire*$^{gfp/gfp}$ thymus were altered compared with those of GFP$^+$ cells containing functional Aire protein from *Aire*$^{+/gfp}$ mouse thymus. First, we noticed that the cell shape of GFP$^+$ mTECs lacking functional Aire protein was altered; in *Aire*$^{gfp/gfp}$ thymus, more GFP$^+$ cells exhibited a globular shape instead of a dendritic to fibroblastic morphology, compared with *Aire*$^{+/gfp}$ thymus (Fig. 2 C, arrows). The lower preponderance of a dendritic shape of GFP$^+$ Aire-less mTECs was verified by statistical analysis. We calculated the level of cell shape complexity for each GFP$^+$ cell by dividing the length of the cellular periphery by the cell area using a computer program (i.e., the higher

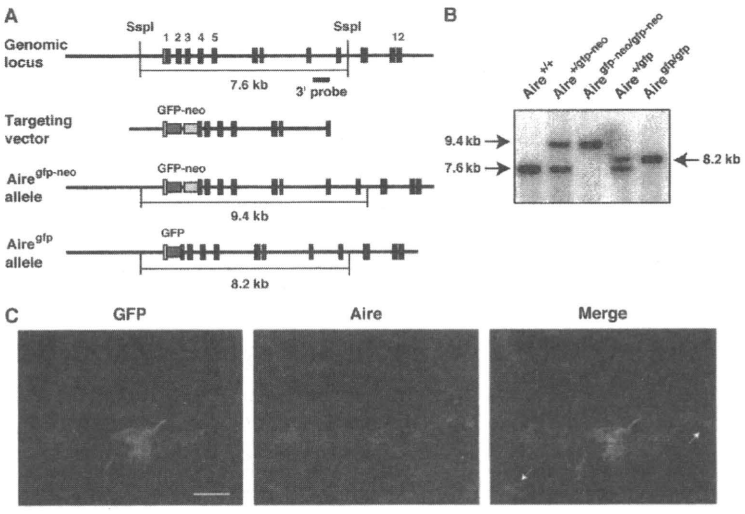

Figure 1. Establishment of Aire/GFP knock-in mice. (A) Targeted insertion of the GFP gene into the *Aire* gene locus by homologous recombination. SspI, *SspI* restriction site. (B) Southern blot analysis of genomic DNA from offspring of Aire/GFP knock-in mice. Tail DNA was digested with *SspI* and hybridized with the 3′ probe shown in A. (C) Concomitant expression of GFP (green) and endogenous mouse Aire (red) assessed by immunohistochemistry of a thymus section from an *Aire*$^{+/gfp}$ mouse. Cells positive for Aire staining but negative for GFP expression are marked with arrows. Bar, 20 µm. One representative experiment from a total of four repeats is shown.

the value, the more complex the cell shape). GFP$^+$ cells from *Aire*$^{gfp/gfp}$ thymus showed lower values (i.e., less complexity per cell) and a narrower distribution of values (i.e., less heterogeneity of cell shape) than those from *Aire*$^{+/gfp}$ thymus (Fig. 2 D). Because a gene-dosage effect has been noticed at the *Aire* gene locus (11), we carefully excluded the possibility that the altered shape of GFP$^+$ cells from *Aire*$^{gfp/gfp}$ thymus was due simply to higher GFP protein expression within each cell, i.e., imposing a potentially toxic burden on the cells. For this purpose, we crossed *Aire*$^{+/gfp}$ mice with *Aire*$^{-/-}$ mice (12) to establish *Aire*$^{-/gfp}$ mice in which the *gfp* allele is single, as in *Aire*$^{+/gfp}$ mice (Fig. S2 A). Similarly to the *Aire*$^{gfp/gfp}$ thymus analysis, GFP$^+$ cells from *Aire*$^{-/gfp}$ thymus demonstrated less complexity of cell shape than those from *Aire*$^{+/gfp}$ thymus, as confirmed using the same method of statistical analysis (Fig. S2 B).

Although we analyzed the thymic organization of *Aire*$^{gfp/gfp}$ mice before the onset of autoimmune pathology (i.e., 4–6 wk after birth), we also excluded the possibility that the altered cell shape of GFP$^+$ cells from *Aire*$^{gfp/gfp}$ thymus was secondary to the autoimmune phenotypes by establishing *Aire*$^{-/gfp}$ mice expressing the OT-II TCR transgene in which the autoreactive T cell repertoire is absent (Fig. S3 A). Morphological changes in GFP$^+$ cells were similarly observed in these mice (Fig. S3 B), suggesting that the altered shape of GFP$^+$ cells lacking Aire protein was independent of autoimmune phenotype.

Second, we noticed that the distribution pattern of mTECs committed to Aire expression was also affected in the absence of functional Aire protein. In contrast with the enrichment of GFP$^+$ cells from *Aire*$^{+/gfp}$ thymus at the cortico-medullary junction, GFP$^+$ cells from *Aire*$^{gfp/gfp}$ thymus tended to be localized

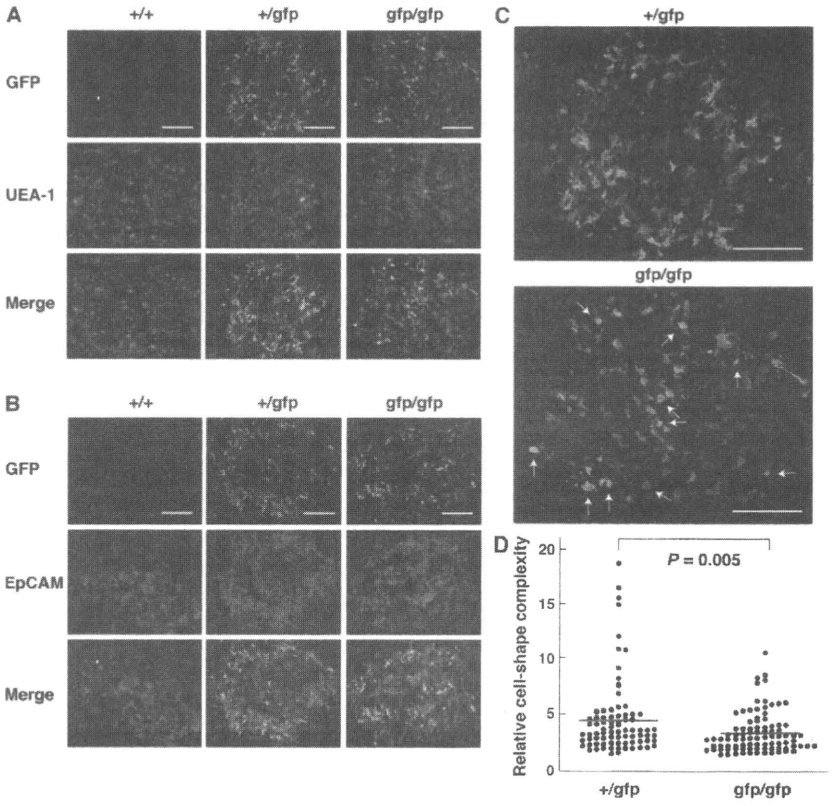

Figure 2. Altered morphology and distribution of mTECs committed to express Aire in the absence of functional Aire protein.
(A and B) mTECs active in *Aire* gene transcription were visualized by immunohistochemistry with anti-GFP Ab (green). The medullary region was identified by staining with UEA-1 (A) or anti-EpCAM mAb (B; red). Bars, 100 µm. One representative experiment from a total of five repeats is shown. (C) Enlargement of the staining with anti-GFP Ab from A for demonstration of altered morphology and distribution of mTECs committed to express Aire in *Aire*$^{gfp/gfp}$ mouse thymus. There were more GFP$^+$ cells with globular shapes (bottom, arrows) in *Aire*$^{gfp/gfp}$ thymus than in *Aire*$^{+/gfp}$ thymus. GFP$^+$ cells from *Aire*$^{+/gfp}$ thymus were enriched at the cortico-medullary junction (top), whereas GFP$^+$ cells from *Aire*$^{gfp/gfp}$ thymus tended to be localized more evenly within each medulla or even enriched at the center of the medulla (bottom). Bars, 100 µm. One representative experiment from a total of five repeats is shown. (D) Morphological changes in the shape of GFP$^+$ cells from *Aire*$^{gfp/gfp}$ mouse thymus demonstrated in C were analyzed statistically. Each circle corresponds to the relative cell shape complexity of a single GFP$^+$ cell calculated with a computer program (see Materials and methods). A total of 80 and 88 GFP$^+$ cells from *Aire*$^{+/gfp}$ and *Aire*$^{gfp/gfp}$ thymi, respectively, were evaluated. Red lines represent mean values. Two mice for each group were analyzed, and similar results were obtained from a total of three repeats.

more uniformly within each medulla or even enriched at the medulla center (Fig. 2 C and Fig. S1 A). Altered distribution of GFP$^+$ Aire-less mTECs was also evident in *Aire*$^{-/gfp}$ mice (Fig. S2 A), as well as in *Aire*$^{-/gfp}$ mice expressing the nonautoreactive OT-II TCR transgene (Fig. S3 A). Collectively, production of a particular mTEC lineage committed to express Aire is not determined by Aire protein alone. However, Aire deficiency in these cells results in morphological changes together with altered location within the medulla, suggesting a role of Aire in the differentiation program of mTECs in a cell-intrinsic manner.

Analysis of embryonic thymus demonstrated that GFP$^+$ cells were absent at embryonic day 13.5, but clearly present at embryonic day 16.5 in both *Aire*$^{+/gfp}$ and *Aire*$^{gfp/gfp}$ mice (Fig. S1 C). Although the effect of absence of Aire protein on the location of GFP$^+$ cells from *Aire*$^{gfp/gfp}$ mice at the embryonic and early P1 (postneonatal) stages was difficult to evaluate because of the less organized thymic structure together with relatively small numbers of GFP$^+$ cells at those stages, morphological alteration of each mTEC committed to Aire expression was already evident at the neonatal stage (P1; Fig. S4 A), as confirmed by the same statistical analysis applied to Fig. 2 D (Fig. S4 B). The properties of GFP$^-$ (i.e., Aire nonexpressing) mTECs as evaluated by immunohistochemistry with UEA-1, anti-EpCAM Ab (Fig. 2, A and B), anti-K5 Ab (Fig. S1 A), ER-TR5 Ab, anti–claudin 3/4 Abs, and MTS10 Ab (not depicted) showed no obvious difference between *Aire*$^{+/gfp}$ and *Aire*$^{gfp/gfp}$ adult thymi.

In addition to the histological evaluation of mTECs based on Aire/GFP expression, another possibility that Aire controls the differentiation program of mTECs has emerged from studies focusing on the cell differentiation markers expressed by mTECs. In the skin, involucrin expression is restricted to postmitotic epithelial cells and serves as a marker of epidermal and follicular terminal differentiation (22). Interestingly, immunohistochemistry of the human thymus using anti-involucrin Ab stains characteristic swirled epithelial structures known as Hassall's corpuscles (23), which is consistent with the fact that Hassall's corpuscles are composed of terminally differentiated mTECs (24). When thymus sections from Aire-sufficient mice were stained with anti-involucrin Ab, involucrin-expressing cells were scattered within the EpCAM$^+$ thymic medulla (Fig. 3 A). The number of involucrin-expressing cells was age dependent and declined between 8 and 11 wk (Fig. 3 B and Table S1, available at http://www.jem.org/cgi/content/full/jem.20080046/DC1). In addition, we occasionally found larger involucrin-expressing structures with a hyalinized degenerated core in the thymic medulla from Aire-sufficient mice, which is reminiscent of Hassall's corpuscles in human thymus (Fig. 3 C). Remarkably, the numbers of mTECs expressing involucrin in Aire-deficient mice were significantly lower than those in Aire-sufficient mice, especially at 4 and 8 wk of age (Fig. 3 B). Furthermore, we observed no typical Hassall's corpuscle-like structures in the thymus of Aire-deficient mice at any age, which is in contrast to those seen in Aire-sufficient mice (Table S1). These results further support the notion that lack of Aire in mTECs alters their differentiation program, thereby altering mTEC integrity.

Next, we used flow cytometric analysis to examine GFP-expressing cells from the thymus. Thymic stromal cells were released enzymatically from adult thymi and stained with anti-CD45 mAb and UEA-1, together with anti-CD80 and anti–MHC class II mAbs. *Aire*$^{+/gfp}$ thymus contained 4.5% UEA-1$^+$GFP$^+$ (i.e., Aire$^+$) cells (from here on simply designated GFP$^+$ cells) in the population of CD45$^-$ stromal cells (Fig. 4 A). When forward scatter (FSC) and side scatter (SSC) parameters were compared between GFP$^+$ cells and UEA-1$^+$GFP$^-$ cells (from here on simply designated GFP$^-$ cells), GFP$^+$ cells were larger and more broadly distributed compared with GFP$^-$ cells (Fig. 4 B, left), suggesting a distinct cellular morphology of Aire$^+$ cells among mTECs. *Aire*$^{gfp/gfp}$ thymus also contained GFP$^+$ cells in the population of CD45$^-$ stromal cells (Fig. 4 A), as already observed by immunohistochemical analysis (Figs. 2 and S1). Interestingly, the proportion of GFP$^+$ cells in *Aire*$^{gfp/gfp}$ thymus was consistently

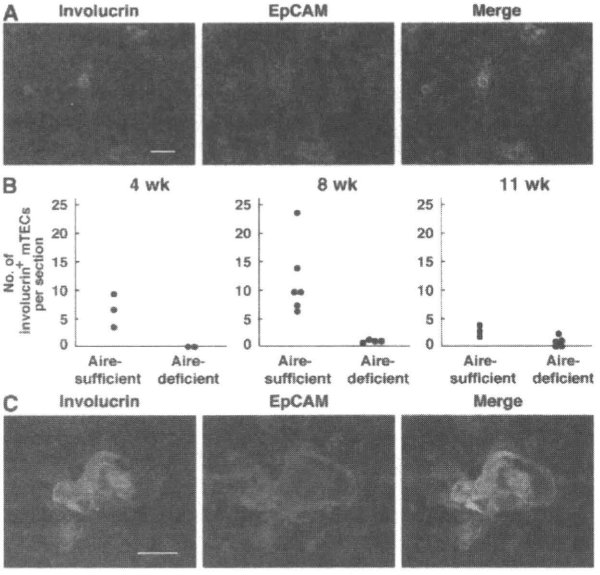

Figure 3. Reduced numbers of terminally differentiated mTECs in the absence of Aire. (A) Involucrin-expressing mTECs (green) were scattered within the thymic medulla (red; stained with anti-EpCAM Ab) of Aire-sufficient mice. Bar, 50 µm. (B) Numbers of involucrin-expressing mTECs were reduced in Aire-deficient mice at 4 (left) and 8 (middle) wk of age. Numbers of involucrin-expressing mTECs in Aire-sufficient mice declined at 11 wk of age (right). Each circle corresponds to the mean number of involucrin-expressing mTECs per section examined in individual mice. Detailed information for the mice examined from a total of five experiments is presented in Table S1 (available at http://www.jem.org/cgi/content/full/jem.20080046/DC1). (C) Hassall's corpuscle-like structures seen in Aire-sufficient mouse thymus stained with anti-involucrin Ab (green) together with anti-EpCAM Ab (red). These discrete and larger involucrin-expressing structures were scarcely detectable in Aire-deficient mouse thymus. Bar, 20 µm. One representative experiment from a total of five repeats is shown.

30–40% higher than in *Aire*$^{+/gfp}$ thymus (Fig. 4 A). Consequently, the ratio of GFP$^+$ cells to GFP$^-$ cells was higher in *Aire*$^{gfp/gfp}$ thymus (~1:5) compared with that in *Aire*$^{+/gfp}$ thymus (~1:10). Although the difference in FSC/SSC parameters between GFP$^+$ and GFP$^-$ cells observed for *Aire*$^{+/gfp}$ mice was also seen in *Aire*$^{gfp/gfp}$ mice (Fig. 4 B, right), FSC/SSC plots of GFP$^+$ cells from *Aire*$^{gfp/gfp}$ mice showed a more condensed profile over a narrower region compared with GFP$^+$ cells from *Aire*$^{+/gfp}$ mice (Fig. 4 B, top), which might reflect the morphological changes in GFP$^+$ mTECs observed by immunohistochemistry (Fig. 2 C). We recorded no GFP expression from CD45$^+$ hematopoietic cells (not depicted) or from CD45$^-$UEA-1$^-$ thymic stromal cells from either *Aire*$^{+/gfp}$ or *Aire*$^{gfp/gfp}$ mice (Fig. 4 A).

We then analyzed the expression of CD80 and MHC class II from each of the populations separated on the basis of GFP expression and UEA-1 binding. GFP$^+$ cells from *Aire*$^{+/gfp}$ mice expressed both CD80 and MHC class II at high levels (CD80^{hi}/class II^{hi}), whereas GFP$^-$ cells from the same animals expressed intermediate to low levels of both CD80 and MHC class II (Fig. 4 C, left). GFP$^+$ cells from *Aire*$^{gfp/gfp}$ thymus were also CD80^{hi}/class II^{hi} (Fig. 4 C, right), indicating that expression of these Ag presentation-related molecules was Aire independent. Indeed, expression levels of both CD80 and MHC class II from GFP$^+$ cells were almost indistinguishable between *Aire*$^{+/gfp}$ and *Aire*$^{gfp/gfp}$ mice when the two flow cytometric profiles were merged (Fig. 4 D, left). However, although difference was small, expression of both CD80 and MHC class II from GFP$^-$ cells from *Aire*$^{gfp/gfp}$ mice was consistently lower than that from *Aire*$^{+/gfp}$ mice (Fig. 4 D, right). This result may indicate that the absence of normal Aire-expressing cells from the medulla is accompanied by phenotypic alteration of Aire-nonexpressing mTECs, which was not evident with the immunohistochemical analysis with the commonly used medullary epithelial cell markers (Fig. 2, A and B; and Fig. S1 A). Collectively, the results suggest that *Aire* deficiency results in a global alteration of the thymic microenvironment that involves not only mTECs committed to express Aire but also the Aire-nonexpressing mTECs that surround Aire$^+$ cells.

Aire-dependent TRA gene expression

Although Aire has been suggested to regulate promiscuous gene expression in mTECs (9, 10), demonstration that Aire$^+$ cells are the major source of promiscuous gene expression from mTECs is still incomplete in the absence of appropriate cell markers for Aire-expressing cell lineages. Existing data for promiscuous gene expression from mTECs were obtained

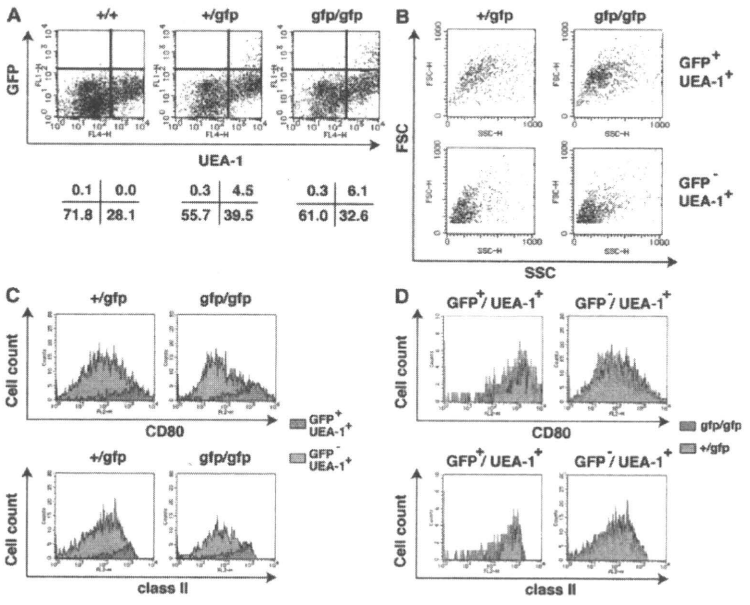

Figure 4. Global alteration of mTEC phenotypes in the absence of Aire. (A) Detection of GFP-expressing cells from thymic stroma by flow cytometric analysis. CD45$^-$ thymic stromal cells were analyzed for the expression of GFP together with binding of UEA-1. Percentages of cells from each fraction are indicated below. (B) mTECs committed to express Aire were larger than mTECs noncommitted to express Aire, irrespective of the presence of Aire protein. FSC/SSC profiles of mTECs committed to express Aire were altered in the absence of functional Aire protein (top). Each FSC/SSC profile was obtained by back gating the corresponding fractions from A based on the expression of GFP and UEA-1. (C) CD80 and MHC class II expression levels were higher in mTECs committed to express Aire than in mTECs noncommitted to express Aire, irrespective of the presence of functional Aire protein. Filled profiles in green and gray are from GFP$^+$ and GFP$^-$ mTECs, respectively. (D) CD80 and MHC class II expression from mTECs committed to express Aire were indistinguishable between *Aire*$^{+/gfp}$ and *Aire*$^{gfp/gfp}$ mice (left) but were reduced in mTECs noncommitted to express Aire in the absence of functional Aire protein (right). Filled profiles in gray and green lines are from *Aire*$^{+/gfp}$ and *Aire*$^{gfp/gfp}$ mice, respectively. Flow cytometric profiles from C were merged for comparison. One representative result from a total of more than five repeats is shown.

by flow cytometric sorting using surrogate Aire$^+$ cell markers such as CD80 and MHC class II. As a result, it is not yet clear which population of mTECs (i.e., Aire-expressing or Aire-nonexpressing mTECs) is deficient in promiscuous gene expression as a result of absence of functional Aire protein. To answer this question, we separated GFP$^+$ and GFP$^-$ mTECs from both *Aire*$^{+/gfp}$ and *Aire*$^{gfp/gfp}$ mice and examined the expression of several TRA genes, including both Aire-dependent (i.e., *insulin 2* and *salivary protein 1* [*SAP1*]) and Aire-independent (*C-reactive protein* [*CRP*]) TRA genes; expression of the former and the latter gene classes has been demonstrated to be reduced or unchanged, respectively, in CD80^{hi}/class II^{hi} Aire-deficient mTECs (9, 10). GFP$^+$ mTECs from *Aire*$^{+/gfp}$ mice showed the highest expression of *insulin 2* and *SAP1*, and expression of those genes was much lower in GFP$^-$ mTECs from the same animals (Fig. 5). Remarkably, both GFP$^+$ and GFP$^-$ mTECs from *Aire*$^{gfp/gfp}$ mice expressed almost none of the Aire-dependent TRA genes *insulin 2* and *SAP1*. mTECs defined by UEA-1 binding from *Aire*$^{+/+}$ mice, which includes both Aire$^+$ and Aire$^-$ cells, showed intermediate expression of those genes. These results clearly indicate two important features of promiscuous gene expression in mTECs. First, Aire$^+$ mTECs are the major cell types responsible for the expression of Aire-dependent TRA genes. Second, mTECs cannot express Aire-dependent TRA genes in the absence of functional Aire protein, even though the lineage commitment to express Aire and the expression of Ag presentation-related molecules, such as CD80 and MHC class II, are preserved (Fig. 4 C). It is important to emphasize that the latter observation does not necessarily mean that Aire acts on the already existing transcriptional machinery required for TRA gene expression within established terminally differentiated mTECs. Rather, in the light of the fact that GFP$^+$ Aire-less mTECs show defective development, as indicated by their altered morphology and distribution, we suggest that Aire$^+$ mTECs acquire their unique machinery for promiscuous gene expression only when they have fully achieved maturation with the help of Aire protein (see Discussion and see Fig. 8).

In marked contrast to Aire-dependent TRA genes, expression of an Aire-independent TRA gene, *CRP*, from GFP$^+$ mTECs was indistinguishable between *Aire*$^{+/gfp}$ and *Aire*$^{gfp/gfp}$ mice. *CRP* expression from GFP$^-$ mTECs was detectable, although the levels were lower than from GFP$^+$ mTECs, and was also similar between *Aire*$^{+/gfp}$ and *Aire*$^{gfp/gfp}$ mice (Fig. 5). As expected, the *Aire* gene was highly expressed from GFP$^+$ mTECs of *Aire*$^{+/gfp}$ mice, although a low level of *Aire* gene expression was detected from GFP$^-$ mTECs, which is possibly a result of slight contamination by cells expressing a trace amount of GFP (i.e., Aire) in this fraction. Expression of the *Aire* gene from both GFP$^+$ and GFP$^-$ cells of *Aire*$^{gfp/gfp}$ mice was at background levels.

Aire-independent TRA gene expression in situ from mTECs

The results in the previous section suggest that individual mTECs do not express a broad array of TRA genes. Rather, each mTEC seems to express a different spectrum of TRA genes. Some TRA genes, such as *insulin 2* and *SAP1* (previously recognized as Aire-dependent genes; references 9, 10), were predominantly expressed from cells of the Aire$^+$ mTEC lineage only when Aire protein was present within the cells, and other TRA genes, such as *CRP* (previously recognized as an Aire-independent gene; references 9, 10), were expressed from both Aire$^+$ and Aire$^-$ mTECs irrespective of the presence of Aire protein. The latter situation was further investigated with the use of GAD67/GFP knock-in mice (*GAD67*$^{+/gfp}$ mice). *GAD67*, an Aire-independent TRA gene that is expressed in the brain and pancreas, is

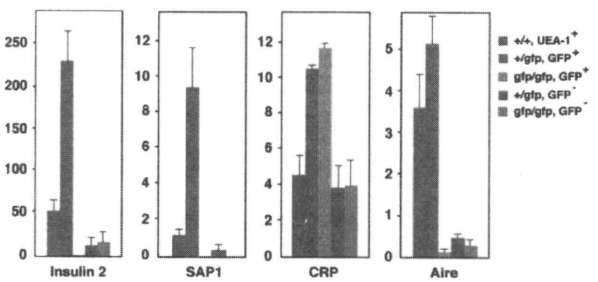

Figure 5. TRA gene expression from mTECs assessed by real-time PCR. Expression of *insulin 2*, *SAP1*, *CRP*, and *Aire* was examined from each fraction of mTECs sorted on the basis of the flow cytometric profile demonstrated in Fig. 4 A. Color bars corresponding to each fraction are indicated on the right. Aire$^+$ mTECs were the major cell types responsible for the expression of Aire-dependent TRA genes (*insulin 2* and *SAP1*), whereas an Aire-independent TRA gene (*CRP*) was expressed from both Aire$^+$ and Aire$^-$ mTECs. Aire expression was assessed to verify the proper sorting of each mTEC fraction. Numbers are relative gene expression level compared with that of the *Hprt* gene. Results are expressed as the mean ± SEM for triplicate wells of one representative experiment from a total of three repeat experiments.

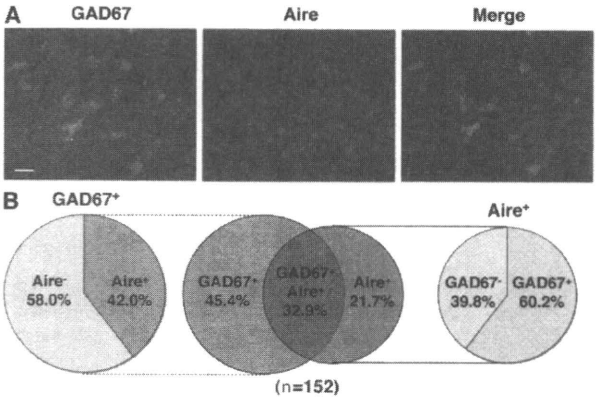

Figure 6. Expression of the Aire-independent TRA gene *GAD67* and of Aire from mTECs in situ. (A) Expression of the *GAD67* gene and Aire was detected by immunohistochemistry with anti-GFP Ab (green) and anti-Aire Ab (red), respectively, in thymus sections from GAD67/GFP knock-in mice. Bar, 20 µm. (B) Results obtained as described for A were calculated for a total of 152 mTECs expressing the *GAD67* gene and/or Aire. One representative experiment from a total of three repeats is shown.

also active in mTECs from *GAD67*$^{+/gfp}$ mice (25). Using immunohistochemistry, we examined the expression of GAD67 together with Aire in *GAD67*$^{+/gfp}$ mouse thymus sections. There were three types of TECs: GAD67^{+}Aire^{-} (45.4%), GAD67^{+}Aire^{+} (32.9%), and GAD67^{-}Aire^{+} (21.7%) (Fig. 6, A and B). Among the GAD67^{+} mTECs, 42.0% expressed Aire and the rest did not (Fig. 6 B), consistent with the Aire-independent nature of *GAD67* gene expression (9, 10). Conversely, among the Aire^{+} mTECs, 60.2% expressed GAD67 and the rest did not, suggesting that Aire expression is not sufficient for TRA expression, at least for this Aire-independent TRA gene.

Expression of *Aire* and Aire-independent TRA genes by nonproliferating mTECs

Previous studies suggested that Aire is predominantly expressed by terminally differentiated cells on the basis of their poor incorporation of BrdU (26, 27). We confirmed this finding by injecting BrdU into *Aire*$^{+/gfp}$ mice. BrdU incorporation was scarce in GFP^{+} mTECs (Fig. 7 A, top). We similarly examined which type of mTECs, immature proliferating or mature nonproliferating, express GAD67 by injecting BrdU into GAD67/GFP knock-in mice. We found that GFP^{+} mTECs incorporated BrdU only weakly (Fig. 7 A, bottom), suggesting that expression of this Aire-independent TRA gene is also imposed on terminally differentiated cells rather on immature proliferating mTECs.

p63 is strongly expressed in epithelial stem cells of the thymus and specifically functions to maintain their extraordinary proliferative capacity (28). To examine whether mTECs expressing the *Aire* and *GAD67* genes have this high proliferative capacity, we examined p63 expression from thymi of Aire/GFP knock-in and GAD67/GFP knock-in adult mice. mTECs expressing GFP from both mouse strains showed little p63 expression by immunohistochemistry (Fig. 7 B), suggesting that neither of these genes is expressed in mTECs with high proliferative capacity. Instead, Aire seems to function within mTECs in the later stages of differentiation, when the cells are also responsible for TRA gene expression.

DISCUSSION

In the present study, we addressed fundamental questions regarding how mTECs acquire the capacity for promiscuous gene expression with the participation of Aire, with the hope that understanding the roles of Aire in thymic organogenesis will help to unravel the molecular mechanisms responsible for expression of immunological self in the thymic microenvironment. The issues include the following: first, whether Aire itself is necessary for the production and/or differentiation

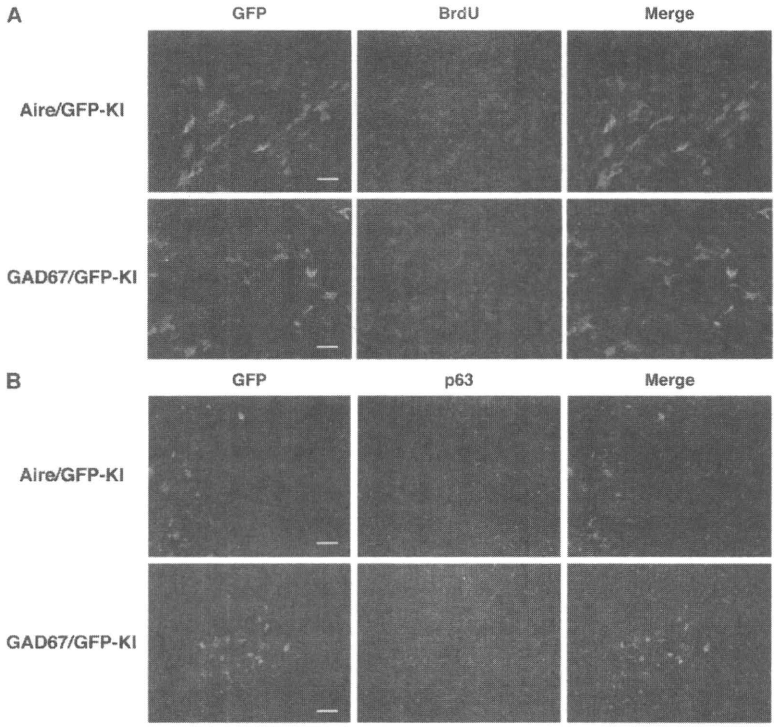

Figure 7. Expression of the *Aire* and *GAD67* genes by nonproliferating mTECs. (A) BrdU incorporation by *Aire*- and *GAD67*-expressing mTECs was evaluated 4 h after i.p. injection of BrdU into *Aire*$^{+/gfp}$ and *GAD67*$^{+/gfp}$ mice, respectively. The thymus sections were stained with anti-GFP (green) and anti-BrdU (red) Abs. Bars, 20 μm. (B) p63 (red) was not detected in mTECs expressing the *Aire* and *GAD67* genes (green). Bars, 40 μm. One representative experiment from a total of four repeats is shown.

program of Aire$^+$ cell lineages; second, whether Aire$^+$ mTECs are necessary for the structural and/or functional organization of other types of mTECs; third, to what extent Aire$^+$ mTECs contribute to the expression of TRA genes; and fourth, the nature of the maturation status of mTECs that express Aire and are responsible for TRA expression. Because Aire-specific Ab cannot be used to investigate the differentiation process of mTECs committed to express Aire in the absence of Aire protein, we established Aire/GFP knock-in mice in which the GFP marker gene was inserted into the *Aire* gene locus in a manner allowing concomitant disruption of functional Aire protein expression. In $Aire^{+/gfp}$ mice, this strategy also enables us to distinguish Aire-expressing cells from Aire-nonexpressing cells without introducing any cell markers incompletely unique to Aire-expressing cells. Accordingly, mTECs committed to Aire expression were faithfully GFP marked with this strategy; mTECs transcriptionally active for the *Aire* gene were mostly positive for staining with anti-Aire Ab by immunohistochemistry. There were, however, small numbers of cells that were either positive for Aire staining but negative for *Aire* gene transcription (i.e., GFP$^-$) or, conversely, positive for *Aire* gene transcription (i.e., GFP$^+$) but negative for Aire staining. The former cell type could result from different half-lives of the two proteins (GFP vs. Aire), whereas the latter cell type could result from Aire protein being present as a diffuse nucleoplasmic form (more difficult to recognize) instead of the typical nuclear-dot form (29). Alternatively, these discrepancies could simply be accounted for by differences in detection sensitivity. Indeed, RT-PCR analysis of flow cytometry–sorted cell fractions showed the expected patterns of *Aire* gene expression.

With Aire/GFP knock-in mice, we have clearly demonstrated that Aire$^+$ mTECs are the major cell types responsible for the expression of so-called Aire-dependent TRA genes such as *insulin 2* and *SAP1* (9, 10). These genes were almost exclusively expressed from GFP$^+$ mTECs of $Aire^{+/gfp}$ mice but not of $Aire^{gfp/gfp}$ mice. In contrast, expression of Aire-independent genes, such as *CRP*, was not affected by the absence of Aire. *CRP* expression from GFP$^+$ cells was similar between $Aire^{+/gfp}$ and $Aire^{gfp/gfp}$ mice. *CRP* expression, although at lower levels, was also observed from GFP$^-$ cells and, again, was indistinguishable between $Aire^{+/gfp}$ and $Aire^{gfp/gfp}$ mice. Expression of *GAD67* in an Aire-independent manner (9, 10) was also supported by immunohistochemistry of GAD67/GFP knock-in thymus, demonstrating *GAD67* expression irrespective of the presence of Aire protein in each mTEC. We speculate that the Aire dependency of TRAs reflects, in part, the cell types in which TRAs are expressed; expression of Aire-dependent genes is confined to Aire$^+$ mTECs, whereas expression of Aire-independent genes occurs from both Aire$^+$ and Aire$^-$ mTECs. It is of note that mTECs do not uniformly express the overlapping spectrum of TRAs, as exemplified by the scattered expression of the *GAD67* gene in GAD67/GFP knock-in mouse thymus. Similarly, although Aire$^+$ mTECs are the major cell types responsible for the expression of Aire-dependent TRA genes, this does not mean that all Aire$^+$ mTECs express Aire-dependent TRA genes uniformly. Indeed, single-cell analysis has demonstrated that expression of Aire in mTECs is not sufficient for simultaneous coexpression of Aire-dependent TRA genes (17). Thus, we favor the notion that promiscuous gene expression reflects the thymus-wide summation of expression of a small number of self-Ags by individual mTECs rather than expression of the complete spectrum of self-Ags by each cell (17, 18).

Because expression of transcription factors associated with developmental plasticity of progenitor cells (i.e., *Nanog*, *Oct4* and *Sox2*) is Aire-dependent in mTECs (18), the developmental model predicts that Aire acts early in the development of mTECs. The developmental model also suggests that promiscuous gene expression represents coordinated gene expression reflecting an alternate program of epithelial differentiation among actively proliferating mTECs at their progenitor or immature stages (19). However, accumulating data together with the results of the present study do not support such a view (26, 27). Rather, it is likely that Aire is acting at the late differentiation stages of mTECs. Accordingly, Aire-dependent processes for achieving promiscuous gene expression might also be active at the late differentiation stages of mTECs (see the subsequent paragraph). Clearly, this does not involve mTECs gaining the ability to express CD80 from CD80^{lo} precursors (30) because GFP$^+$ mTECs from $Aire^{gfp/gfp}$ mice demonstrated normal levels of CD80 expression. It is necessary to dissect the developmental process of mTECs, thereby precisely identifying the Aire-dependent steps of mTEC differentiation.

Given that Aire-expressing cells are terminally differentiated, the demonstration that Aire$^+$ mTECs are the major cell types responsible for expression of TRA genes, at least for Aire-dependent genes, apparently favors the terminal differentiation model for Aire-dependent promiscuous gene expression from mTECs (7, 10, 11). However, our results do support a key aspect of a role for Aire in the developmental model (17–19): absence of Aire in mTECs causes morphological changes together with altered distribution of mTECs committed to express Aire. Indeed, the difference in appearance of GFP-expressing cells was distinct enough to allow discrimination between $Aire^{+/gfp}$ and $Aire^{gfp/gfp}$ mouse sections by blind analysis. Interestingly, Gillard et al. (18) noted that globular mTECs without visible cellular projections were more prominent in Aire-deficient thymus, which could represent the GFP$^+$ globular mTECs we observed in $Aire^{gfp/gfp}$ mice. Furthermore, expression of functional molecules, such as CD80 and MHC class II from mTECs noncommitted to express Aire, was also affected by the absence of Aire, suggesting that Aire and/or Aire$^+$ mTECs influence the organization of mTECs beyond simply controlling promiscuous gene expression within Aire-expressing cell lineages. We do not believe that the demonstration that terminally differentiated Aire-expressing cells are the major source of promiscuous gene expression (apparently favoring the terminal differentiation model) and the demonstration that Aire and/or Aire$^+$ cells controls thymic organogenesis (consistent with the developmental model; reference 18 and present study) are mutually exclusive. Instead,

Aire could both promote the differentiation program of mTECs committed to express Aire, ensuring that they become fully equipped with the necessary machinery for promiscuous gene expression, and be an efficient driver of promiscuous gene expression in such cells. Thus, promiscuous gene expression seems to be accomplished in terminally differentiated mTECs that have matured in the presence of Aire protein (Fig. 8). Alternatively, Aire might be necessary for maintenance of a terminally differentiated state in which mTECs manifest a dendritic shape with fully competent promiscuous gene expression.

We found that the numbers of mTECs expressing involucrin, a marker of epidermal differentiation (22), were reduced in Aire-deficient mouse thymus. It was noteworthy that involucrin-expressing mTECs themselves were negative for Aire expression with immunohistochemistry (unpublished data), thus making it unlikely that *involucrin* gene expression in mTECs is under direct transcriptional control by Aire as a part of TRA gene expression. Similarly, it is unknown whether impaired involucrin expression is specific to mTECs committed to Aire expression or whether lack of Aire$^+$ mTECs affects the differentiation of other type(s) of mTECs that would otherwise express involucrin at their terminally differentiated stages. Based on the fact that GFP$^+$ Aire-less mTECs showed alterations in their morphology as well as distribution, we assume that the former possibility is more likely. Interestingly, we found that reduction of involucrin-expressing mTECs in Aire-deficient mice was associated with a nearly absence of Hassall's corpuscle-like structures, although the exact relevance of this phenotype to the breakdown of central tolerance in Aire-deficient mice remains unknown (31). Together with the fact that formation of thymic cysts is a predominant feature of Aire-deficient mice (18, 26), it seems likely that Aire exerts more global control of the differentiation program of mTECs than was initially thought.

Finally, although we have demonstrated that Aire organizes the global mTEC integrity that facilitates promiscuous gene expression in the thymic microenvironment, the exact nature of the mTEC differentiation program under the control of Aire protein still remains unknown. We have demonstrated that both *Aire* and an Aire-independent TRA gene, *GAD67*, are predominantly expressed by nonproliferative cells, although we cannot completely exclude the possibility that expression of these genes is associated with immature cells that turn over slowly and, thus, would be poorly labeled by BrdU. The results prompt us to propose a fascinating hypothesis that promiscuous gene expression is achieved by induction of heterogeneity among terminally differentiated mTECs rather than by multipotentiality of mTEC progenitors. We speculate that Aire may contribute to mTEC heterogeneity by acting on mTECs at the late differentiation stages and that lack of Aire may result in failure to create this heterogeneity. According to this scenario, additional mechanisms for the development of Aire-dependent autoimmunity might be possible beyond reduced TRA expression from Aire-deficient mTECs, for instance, altered Ag processing and/or presentation capacity by Aire-deficient mTECs (12) and/or altered T cell development affecting establishment of the complete T cell repertoire. Study of the mechanisms underlying the Aire-dependent production of heterogeneity among mature mTECs might be a rewarding approach to elucidating the nature of the negative selection niche in the thymus.

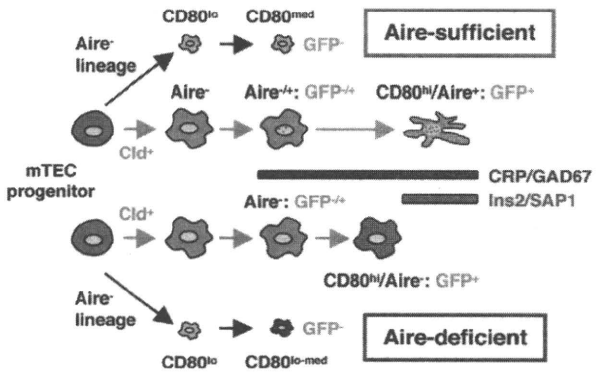

Figure 8. Schematic representation of the roles of Aire in mTEC differentiation and TRA gene expression. Aire-expressing cell lineages develop from mTEC progenitor cells through concomitant expression of claudin (26). Expression of Aire-dependent TRA genes, such as *insulin 2* and *SAP1*, can be accomplished in terminally differentiated mTECs showing a dendritic to fibroblastic morphology that have fully matured with the help of Aire protein (marked as Aire-sufficient). Lack of Aire in mTECs results in premature termination of differentiation, although claudin$^+$ Aire-expressing cell lineages can still develop and pass the CD80-expressing maturation stage (marked as Aire-deficient). These CD80^{hi} Aire-less mTECs have a more globular cell shape and lack transcriptional machinery for Aire-dependent TRA genes. Because Aire-independent TRA genes, such as *CRP* and *GAD67*, can be expressed before the terminal differentiation stages, lack of Aire has little impact on their expression. The possibility also remains that Aire is necessary for the maintenance of a terminally differentiated state, in which mTECs manifest a dendritic shape with fully competent promiscuous gene expression.

MATERIALS AND METHODS

Mice. Aire/GFP knock-in mice (RIKEN Center for Developmental Biology accession No. CDB0483K) were generated by gene targeting as described previously (32). In brief, the targeting vector was constructed by replacing the genomic *Aire* locus starting from exon 1 (immediately after the Kozak sequence) to exon 2 with a GFP-neomycin resistance (neo^r) gene cassette (20). The neo^r gene cassette harbors loxP sites at both ends. The targeting vector was introduced into TT2 embryonic stem cells (33), and the homologous recombinant clones were first identified by PCR and confirmed by Southern blot analysis. After the targeted cells had been injected into morula-stage embryos, the resulting chimeric male mice were mated with C57BL/6 females (CLEA) to establish germ-line transmission. *Aire*$^{+/gfp\text{-}neo}$ mice were crossed with Ayu1-Cre mice (21), a general deleter Cre recombinase-expressing transgenic line, to remove the neo^r gene cassette. After confirming removal of the neo^r gene cassette, mice were crossed with C57BL/6 mice to select the line containing the GFP knock-in allele but not the Cre recombinase-expressing transgene. *Aire*$^{+/gfp}$ mice were then crossed to obtain *Aire*$^{gfp/gfp}$ mice, which have the null mutation for the *Aire* gene. GAD67/GFP knock-in mice were heterozygous for GAD67-GFP (Δneo) as described previously (34). OT-II transgenic mice (35) were purchased from The Jackson Laboratory. The mice were maintained under pathogen-free conditions.

The protocols used in this study were in accordance with the Guidelines for Animal Experimentation of Tokushima University School of Medicine and were conducted with the approval of the RIKEN Kobe Animal Experiment Committee.

Immunohistochemistry. Mice were killed and the thymus tissues were fixed as described previously (25, 36). Immunohistochemical analysis of the thymus with UEA-1 (Vector Laboratories), rat anti-EpCAM mAb (BD), and rabbit polyclonal anti-K5 Ab (Covance) was performed as described previously (37). Rabbit polyclonal anti-Aire Ab was produced as described previously (13). Goat polyclonal anti-GFP Ab (Novus Biologicals) and rabbit polyclonal anti-GFP Ab (Invitrogen) were used for the detection of GFP-expressing cells. BrdU incorporation by mTECs was examined 4 h after i.p. injection of 1 mg BrdU/mouse, and the detection of BrdU incorporation was performed with anti-BrdU Ab (BD), as described previously (26). Rabbit polyclonal anti-p63 Ab was purchased from Santa Cruz Biotechnology, Inc. The level of cell shape complexity for each GFP^+ cell was calculated by dividing the length of the cellular periphery by the cell area (i.e., periphery/area $\times$ $1/4\pi$) measured by the WinROOF program (Mitani Corporation). After obtaining photos of the thymus sections stained with anti-GFP Ab, the photos were subjected to analysis with the software. Immunohistochemistry of the thymus sections and statistical analysis of cell shape complexity from different genotype of mice for comparison were processed simultaneously in the same set of experiment to minimize variability between the assays. Numbers of involucrin-expressing mTECs were assessed after staining the thymus sections with rabbit polyclonal Ab against mouse involucrin (Covance). Well developed $EpCAM^+$ thymic medullas were examined for the presence of involucrin-expressing cells from several thymus sections obtained from individual mice.

TEC preparation and flow cytometric analysis. TECs were prepared as described previously (12). In brief, thymic lobes were isolated from mice and cut into small pieces. The fragments were gently rotated in RPMI 1640 medium (Invitrogen) supplemented with 10% heat-inactivated FCS (Invitrogen), 20 mM Hepes, 100 U/ml penicillin, 100 μg/ml streptomycin, and 50 μM 2-ME at 4°C for 30 min and dispersed further with pipetting to remove the majority of thymocytes. The resulting thymic fragments were digested with 0.125% collagenase D (Roche) and 10 U/ml DNase I (Roche) in RPMI 1640 at 37°C for 15 min. The supernatants, containing dissociated TECs, were saved, and the remaining thymic fragments were further digested with collagenase D and DNase I. This step was repeated twice, and the remaining thymic fragments were digested with 0.125% collagenase/dispase (Roche) and DNase I at 37°C for 30 min. The supernatants from this digest were combined with the supernatants from the collagenase digests, and the mixture was centrifuged for 5 min at 450 *g*. The cells were suspended in PBS, containing 5 mM EDTA and 0.5% FCS, and kept on ice until the staining. The cells were stained with anti-CD45 mAb (BD) and UEA-1 and subjected to flow cytometric cell sorting with a FACS Vantage (BD). Flow cytometric analysis was performed after staining the cells with anti-CD45 mAb, UEA-1, anti-I-A^b (eBioscience), and anti-CD80 (eBioscience) mAbs with a FACSCalibur (BD) as described previously (13, 37).

Real-time PCR. RNA was extracted from sorted mTECs with RNeasy Mini kits (QIAGEN) and made into cDNA with cDNA Cycle kits (Invitrogen) according to the manufacturer's instructions. Real-time PCR for quantification of the *insulin 2*, *SAP1*, *CRP*, and *Hprt* genes was performed as described previously (12, 13). The primers and the probes are as follows: *insulin 2* primers, 5′-AGACCATCAGCAAGCAGGTC-3′ and 5′-CTGGTGCAGCACTGATCCAC-3′; *insulin 2* probe, 5′-FAM-CCCGGCAGAAGCGTGGCATT-3′; *SAP1* primers, 5′-ACTCCTTGTGTTGCTTGGTGTTT-3′ and 5′-TCGACTGAATCAGAGGAATCAACT-3′; *SAP1* probe, 5′-FAM-TTCACCAGCAGAATCAGCAGTTCCAGAA-3′; *CRP* primers, 5′-TACTCTGGTGCCTTCTGATCATGA-3′ and 5′-GGCTTCTTTGACTCTGCTTCCA-3′; *CRP* probe, 5′-FAM-CAGCTTCTCTCGGACTTTTGGTCATGA-3′; *Hprt* primers, 5′-TGAAGAGCTACTGTAATGATCAGTCAAC-3′ and 5′-AGCAAGCTTGCAACCTTAACCA-3′; and *Hprt* probe, 5′-FAM-TGCTTTCCCTGGTTAAGCAGTACAGCCC-3′.

Statistical analysis. All results are expressed as mean ± SEM. Statistical analysis was performed using Student's two-tailed unpaired *t* test for comparisons between two groups. Differences were considered significant if p-values were 0.05 or less.

Online supplemental materials. Fig. S1 shows Aire-expressing cells in adult and embryonic thymi. Fig. S2 shows altered morphology together with the distribution of GFP^+ Aire-less mTECs in $Aire^{-/gfp}$ mice. Fig. S3 shows altered morphology together with the distribution of GFP^+ Aire-less mTECs in $Aire^{-/gfp}$ mice expressing the nonautoreactive OT-II TCR transgene. Fig. S4 shows altered morphology of GFP^+ Aire-less mTECs in $Aire^{gfp/gfp}$ mice at neonatal stage P1. Table S1 shows detailed information for mice analyzed for involucrin-expressing mTECs. Online supplemental material is available at http://www.jem.org/cgi/content/full/jem.20080046/DC1.

We thank Drs. Y. Hamazaki, E.A. Robey and A.G. Farr for suggestions on immunohistochemistry.

This work was supported in part by Grants-in-Aid for Scientific Research from the Japan Society for the Promotion of Science and from the Ministry of Education, Culture, Sports, Science and Technology of Japan, and by Health and Labor Sciences Research Grants, Research on Psychiatric and Neurological Diseases and Mental Health (M. Matsumoto).

The authors have no conflicting financial interests.

Submitted: 7 January 2008
Accepted: 17 October 2008

REFERENCES

1. Kamradt, T., and N.A. Mitchison. 2001. Tolerance and autoimmunity. *N. Engl. J. Med.* 344:655–664.
2. Björses, P., J. Aaltonen, N. Horelli-Kuitunen, M.L. Yaspo, and L. Peltonen. 1998. Gene defect behind APECED: a new clue to autoimmunity. *Hum. Mol. Genet.* 7:1547–1553.
3. Pitkänen, J., and P. Peterson. 2003. Autoimmune regulator: from loss of function to autoimmunity. *Genes Immun.* 4:12–21.
4. Björses, P., M. Pelto-Huikko, J. Kaukonen, J. Aaltonen, L. Peltonen, and I. Ulmanen. 1999. Localization of the APECED protein in distinct nuclear structures. *Hum. Mol. Genet.* 8:259–266.
5. Heino, M., P. Peterson, J. Kudoh, K. Nagamine, A. Lagerstedt, V. Ovod, A. Ranki, I. Rantala, M. Nieminen, J. Tuukkanen, et al. 1999. Autoimmune regulator is expressed in the cells regulating immune tolerance in thymus medulla. *Biochem. Biophys. Res. Commun.* 257:821–825.
6. Hogquist, K.A., T.A. Baldwin, and S.C. Jameson. 2005. Central tolerance: learning self-control in the thymus. *Nat. Rev. Immunol.* 5:772–782.
7. Kyewski, B., and L. Klein. 2006. A central role for central tolerance. *Annu. Rev. Immunol.* 24:571–606.
8. Derbinski, J., A. Schulte, B. Kyewski, and L. Klein. 2001. Promiscuous gene expression in medullary thymic epithelial cells mirrors the peripheral self. *Nat. Immunol.* 2:1032–1039.
9. Anderson, M.S., E.S. Venanzi, L. Klein, Z. Chen, S.P. Berzins, S.J. Turley, H. von Boehmer, R. Bronson, A. Dierich, C. Benoist, and D. Mathis. 2002. Projection of an immunological self shadow within the thymus by the aire protein. *Science.* 298:1395–1401.
10. Derbinski, J., J. Gabler, B. Brors, S. Tierling, S. Jonnakuty, M. Hergenhahn, L. Peltonen, J. Walter, and B. Kyewski. 2005. Promiscuous gene expression in thymic epithelial cells is regulated at multiple levels. *J. Exp. Med.* 202:33–45.
11. Liston, A., D.H. Gray, S. Lesage, A.L. Fletcher, J. Wilson, K.E. Webster, H.S. Scott, R.L. Boyd, L. Peltonen, and C.C. Goodnow. 2004. Gene dosage–limiting role of *Aire* in thymic expression, clonal deletion, and organ-specific autoimmunity. *J. Exp. Med.* 200:1015–1026.
12. Kuroda, N., T. Mitani, N. Takeda, N. Ishimaru, R. Arakaki, Y. Hayashi, Y. Bando, K. Izumi, T. Takahashi, T. Nomura, et al. 2005. Development

of autoimmunity against transcriptionally unrepressed target antigen in the thymus of Aire-deficient mice. *J. Immunol.* 174:1862–1870.
13. Niki, S., K. Oshikawa, Y. Mouri, F. Hirota, A. Matsushima, M. Yano, H. Han, Y. Bando, K. Izumi, M. Matsumoto, et al. 2006. Alteration of intra-pancreatic target-organ specificity by abrogation of Aire in NOD mice. *J. Clin. Invest.* 116:1292–1301.
14. Anderson, M.S., E.S. Venanzi, Z. Chen, S.P. Berzins, C. Benoist, and D. Mathis. 2005. The cellular mechanism of Aire control of T cell tolerance. *Immunity.* 23:227–239.
15. Devoss, J., Y. Hou, K. Johannes, W. Lu, G.I. Liou, J. Rinn, H. Chang, R. Caspi, L. Fong, and M.S. Anderson. 2006. Spontaneous autoimmunity prevented by thymic expression of a single self-antigen. *J. Exp. Med.* 203:2727–2735.
16. Matsumoto, M. 2007. Transcriptional regulation in thymic epithelial cells for the establishment of self tolerance. *Arch. Immunol. Ther. Exp. (Warsz.).* 55:27–34.
17. Gillard, G.O., and A.G. Farr. 2006. Features of medullary thymic epithelium implicate postnatal development in maintaining epithelial heterogeneity and tissue-restricted antigen expression. *J. Immunol.* 176:5815–5824.
18. Gillard, G.O., J. Dooley, M. Erickson, L. Peltonen, and A.G. Farr. 2007. Aire-dependent alterations in medullary thymic epithelium indicate a role for Aire in thymic epithelial differentiation. *J. Immunol.* 178:3007–3015.
19. Gillard, G.O., and A.G. Farr. 2005. Contrasting models of promiscuous gene expression by thymic epithelium. *J. Exp. Med.* 202:15–19.
20. Moriguchi, T., M. Hamada, N. Morito, T. Terunuma, K. Hasegawa, C. Zhang, T. Yokomizo, R. Esaki, E. Kuroda, K. Yoh, et al. 2006. MafB is essential for renal development and F4/80 expression in macrophages. *Mol. Cell. Biol.* 26:5715–5727.
21. Niwa, H., K. Araki, S. Kimura, S. Taniguchi, S. Wakasugi, and K. Yamamura. 1993. An efficient gene-trap method using poly A trap vectors and characterization of gene-trap events. *J. Biochem.* 113:343–349.
22. Fuchs, E. 1990. Epidermal differentiation. *Curr. Opin. Cell Biol.* 2:1028–1035.
23. Hale, L.P., and M.L. Markert. 2004. Corticosteroids regulate epithelial cell differentiation and Hassall body formation in the human thymus. *J. Immunol.* 172:617–624.
24. Patel, D.D., L.P. Whichard, G. Radcliff, S.M. Denning, and B.F. Haynes. 1995. Characterization of human thymic epithelial cell surface antigens: phenotypic similarity of thymic epithelial cells to epidermal keratinocytes. *J. Clin. Immunol.* 15:80–92.
25. Maemura, K., Y. Yanagawa, K. Obata, T. Dohi, Y. Egashira, Y. Shibayama, and M. Watanabe. 2006. Antigen-presenting cells expressing glutamate decarboxylase 67 were identified as epithelial cells in glutamate decarboxylase 67-GFP knock-in mouse thymus. *Tissue Antigens.* 67:198–206.
26. Hamazaki, Y., H. Fujita, T. Kobayashi, Y. Choi, H.S. Scott, M. Matsumoto, and N. Minato. 2007. Medullary thymic epithelial cells expressing Aire represent a unique lineage derived from cells expressing claudin. *Nat. Immunol.* 8:304–311.
27. Gray, D., J. Abramson, C. Benoist, and D. Mathis. 2007. Proliferative arrest and rapid turnover of thymic epithelial cells expressing Aire. *J. Exp. Med.* 204:2521–2528.
28. Senoo, M., F. Pinto, C.P. Crum, and F. McKeon. 2007. p63 Is essential for the proliferative potential of stem cells in stratified epithelia. *Cell.* 129:523–536.
29. Akiyoshi, H., S. Hatakeyama, J. Pitkänen, Y. Mouri, V. Doucas, J. Kudoh, K. Tsurugaya, D. Uchida, A. Matsushima, K. Oshikawa, et al. 2004. Subcellular expression of autoimmune regulator (AIRE) is organized in a spatiotemporal manner. *J. Biol. Chem.* 279:33984–33991.
30. Rossi, S.W., M.Y. Kim, A. Leibbrandt, S.M. Parnell, W.E. Jenkinson, S.H. Glanville, F.M. McConnell, H.S. Scott, J.M. Penninger, E.J. Jenkinson, et al. 2007. RANK signals from $CD4^+3^-$ inducer cells regulate development of Aire-expressing epithelial cells in the thymic medulla. *J. Exp. Med.* 204:1267–1272.
31. Liu, Y.J. 2006. A unified theory of central tolerance in the thymus. *Trends Immunol.* 27:215–221.
32. Murata, T., K. Furushima, M. Hirano, H. Kiyonari, M. Nakamura, Y. Suda, and S. Aizawa. 2004. *ang* is a novel gene expressed in early neuroectoderm, but its null mutant exhibits no obvious phenotype. *Gene Expr. Patterns.* 5:171–178.
33. Yagi, T., T. Tokunaga, Y. Furuta, S. Nada, M. Yoshida, T. Tsukada, Y. Saga, N. Takeda, Y. Ikawa, and S. Aizawa. 1993. A novel ES cell line, TT2, with high germline-differentiating potency. *Anal. Biochem.* 214:70–76.
34. Tamamaki, N., Y. Yanagawa, R. Tomioka, J. Miyazaki, K. Obata, and T. Kaneko. 2003. Green fluorescent protein expression and colocalization with calretinin, parvalbumin, and somatostatin in the GAD67-GFP knock-in mouse. *J. Comp. Neurol.* 467:60–79.
35. Barnden, M.J., J. Allison, W.R. Heath, and F.R. Carbone. 1998. Defective TCR expression in transgenic mice constructed using cDNA-based alpha- and beta-chain genes under the control of heterologous regulatory elements. *Immunol. Cell Biol.* 76:34–40.
36. Kusser, K.L., and T.D. Randall. 2003. Simultaneous detection of EGFP and cell surface markers by fluorescence microscopy in lymphoid tissues. *J. Histochem. Cytochem.* 51:5–14.
37. Kajiura, F., S. Sun, T. Nomura, K. Izumi, T. Ueno, Y. Bando, N. Kuroda, H. Han, Y. Li, A. Matsushima, et al. 2004. NF-κB-inducing kinase establishes self-tolerance in a thymic stroma-dependent manner. *J. Immunol.* 172:2067–2075.

LETTERS

Innate production of T_H2 cytokines by adipose tissue-associated c-Kit$^+$Sca-1$^+$ lymphoid cells

Kazuyo Moro[1,4], Taketo Yamada[2], Masanobu Tanabe[3], Tsutomu Takeuchi[3], Tomokatsu Ikawa[5], Hiroshi Kawamoto[5], Jun-ichi Furusawa[1], Masashi Ohtani[1,6], Hideki Fujii[1] & Shigeo Koyasu[1,7]

Innate immune responses are important in combating various microbes during the early phases of infection. Natural killer (NK) cells are innate lymphocytes that, unlike T and B lymphocytes, do not express antigen receptors but rapidly exhibit cytotoxic activities against virus-infected cells and produce various cytokines[1,2]. Here we report a new type of innate lymphocyte present in a novel lymphoid structure associated with adipose tissues in the peritoneal cavity. These cells do not express lineage (Lin) markers but do express c-Kit, Sca-1 (also known as Ly6a), IL7R and IL33R. Similar lymphoid clusters were found in both human and mouse mesentery and we term this tissue 'FALC' (fat-associated lymphoid cluster). FALC Lin$^-$c-Kit$^+$Sca-1$^+$ cells are distinct from lymphoid progenitors[3] and lymphoid tissue inducer cells[4]. These cells proliferate in response to IL2 and produce large amounts of T_H2 cytokines such as IL5, IL6 and IL13. IL5 and IL6 regulate B-cell antibody production and self-renewal of B1 cells[5–7]. Indeed, FALC Lin$^-$c-Kit$^+$Sca-1$^+$ cells support the self-renewal of B1 cells and enhance IgA production. IL5 and IL13 mediate allergic inflammation and protection against helminth infection[8,9]. After helminth infection and in response to IL33, FALC Lin$^-$c-Kit$^+$Sca-1$^+$ cells produce large amounts of IL13, which leads to goblet cell hyperplasia—a critical step for helminth expulsion. In mice devoid of FALC Lin$^-$c-Kit$^+$Sca-1$^+$ cells, such goblet cell hyperplasia was not induced. Thus, FALC Lin$^-$c-Kit$^+$Sca-1$^+$ cells are T_H2-type innate lymphocytes, and we propose that these cells be called 'natural helper cells'.

The cytokine receptor common γ chain (γ_c) is critical for the differentiation of lymphocytes as well as lymphoid tissue inducer (LTi) cells. The latter have an essential role in the development of lymphoid tissues such as lymph nodes, Peyer's patches and isolated lymphoid follicles[10,11]. Herein we identified a previously unrecognized γ_c-dependent lymphoid structure in mouse. Clusters of lymphocytes were observed along the blood vessels in the mouse mesentery—an adipose tissue in the peritoneal cavity (Fig. 1a, b). These clusters were surrounded by adipose tissues (Fig. 1c), and 5–50 clusters were found throughout the mesentery. The size of each cluster was 100–500 μm in diameter, and the number and size of clusters increased with age. Although lymphocytes were the dominant cell population in the cluster, unlike lymph nodes, no fibrous capsule was present around the clusters, and lymphocytes were in direct contact with ambient adipocytes (Supplementary Fig. 1a). The blood capillaries in these clusters were filled with lymphocytes and a few red blood cells (Supplementary Fig. 1b).

Flow cytometric analysis (Fig. 1d) identified a cell population expressing c-Kit and Sca-1 but no Lin markers (CD3ε, CD4, CD8α, TCRβ, TCRδ, CD5, CD19, B220 (encoded by *Ptprc*), NK1.1 (Klrb1c), Ter119 (Ly76), Gr-1 (Ly6g), Mac-1 (Itgam), CD11c (Itgax) and FcεRIα) that

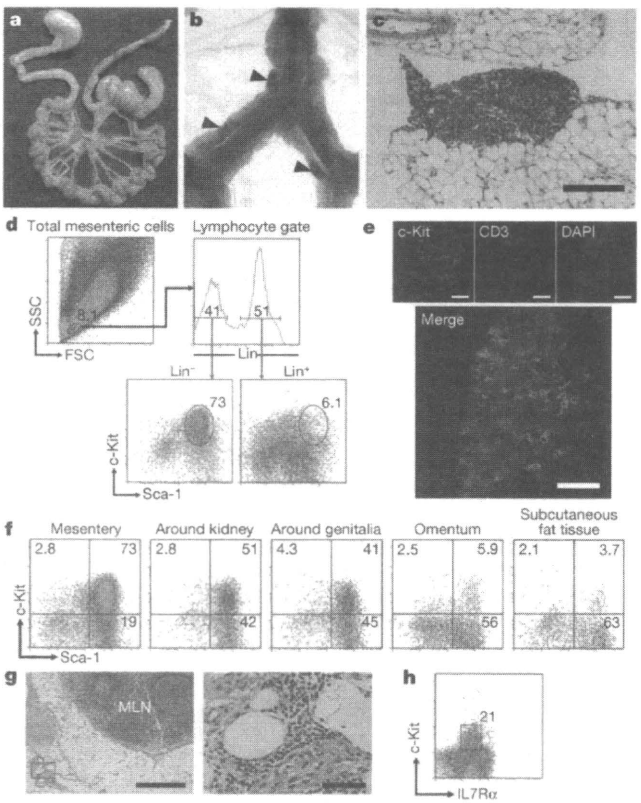

Figure 1 | Lin$^-$c-Kit$^+$Sca-1$^+$ cells exist in FALCs. **a**, Photograph of mouse mesentery (framed by green line). **b**, A higher magnification of the area framed by the yellow square in **a** after staining with 0.5% toluidine blue. Arrowheads indicate mesenteric lymph nodes (MLN) in **a** and the lymphoid clusters in **b**. **c**, Haematoxylin and eosin (H&E)-stained specimen of a lymphoid cluster in the mesentery. Scale bar, 200 μm. **d**, Flow cytometry of mesenteric cells stained with antibodies against Lin, c-Kit and Sca-1. FSC, forward scatter; SSC, side scatter. **e**, Immunofluorescence staining of a lymphoid cluster. DAPI, 4′,6-diamidino-2-phenylindole. Scale bars, 50 μm. **f**, Flow cytometry of cells isolated from the indicated adipose tissues. **g**, H&E staining of human mesentery. Left: scale bar, 1 mm. Right: a higher magnification photograph of the area framed by the red square in the left panel. Scale bar, 100 μm. **h**, Flow cytometry of human mesenteric cells stained with c-Kit and IL7Rα.

[1]Department of Microbiology and Immunology, [2]Department of Pathology, [3]Department of Tropical Medicine and Parasitology, Keio University School of Medicine, Shinjuku-ku, Tokyo 160-8582, Japan. [4]Japan Science and Technology Agency (JST), CREST, Chiyoda-ku, Tokyo 102-0075, Japan. [5]Laboratory for Lymphocyte Development, Riken Research Center for Allergy and Immunology, Yokohama, Kanagawa 230-0045, Japan. [6]Department of Cell Signalling, Institute of Biomedical Science, Kansai Medical University, Moriguchi, Osaka 570-8506, Japan. [7]Research Center for Science Systems, Japan Society for the Promotion of Science (JSPS), Chiyoda-ku, Tokyo 102-8472, Japan.

made up 20–40% of total lymphocytes in mesenteric cells, comprising 0.5–2 × 10^5 cells per mouse. The clusters contained c-Kit$^+$ cells interspersed with CD3$^+$ T cells and B220$^+$ B cells (Fig. 1e and Supplementary Fig. 2a). Lin$^-$c-Kit$^+$Sca-1$^+$ cells were also found in adipose tissues around the kidney and genitalia, but very few were found in the subcutaneous fat tissue or omentum (Fig. 1f). Hence, we named these lymphoid clusters 'fat-associated lymphoid clusters' or FALCs. The structure of FALCs is similar to that of omental milky spots[12] in that both contain lymphocytes framed by adipose tissue in the peritoneal cavity. However, milky spots contain T- and B-cell zones but few c-Kit$^+$Sca-1$^+$ cells (Fig. 1f and Supplementary Fig. 2). Similar lymphocyte clusters distinct from lymph nodes were found in the human mesentery (Fig. 1g). Human FALCs contained a clearly evident cell population expressing c-Kit and IL7Rα (Fig. 1h).

Giemsa staining showed that FALC c-Kit$^+$Sca-1$^+$ cells were small in size and had a round shape, dark nucleus and scanty cytoplasm (Fig. 2a)—all characteristics of lymphoid cells. Electron microscopy confirmed a high nucleus/cytoplasm ratio and scanty cytoplasm, and also showed a poorly developed Golgi apparatus and endoplasmic reticulum (Fig. 2b). FALC c-Kit$^+$Sca-1$^+$ cells expressed CD45 (encoded by *Ptprc*), IL7Rα, Thy-1.2 (Thy1), CD27, T1/ST2 (IL1RL1, a subunit of IL33R)[13] and activation markers such as CD25 (IL2RA), CD38, CD44, CD69 and GITR (Tnfrsf18) (Fig. 2c). This population was present in *Rag2*$^{-/-}$ and *nu/nu* mice but absent from *gc*$^{-/-}$ (also known as *Il2rg*$^{-/-}$) and *Il7*$^{-/-}$ mice (Fig. 2d), indicating that this population is probably of lymphoid lineage with differentiation dependent on IL7. Culturing FALC c-Kit$^+$Sca-1$^+$ cells on TSt-4/DLL1, a thymic stroma cell line expressing delta-like 1 (DLL1), which supports the development of T-cell progenitors to mature T cells[14], did not induce T-cell differentiation (Supplementary Fig. 3). FALC c-Kit$^+$Sca-1$^+$ cells also did not differentiate into B cells when co-cultured with TSt-4 cells (Supplementary Fig. 3). Furthermore, no differentiation of NK cells or the recently identified NK1.1$^+$NKp46$^+$ cells producing IL22 (ref. 15) was observed either *in vitro* or *in vivo* (data not shown). FALC c-Kit$^+$Sca-1$^+$ cells are also phenotypically similar to LTi cells[4]. As shown in Fig. 2d, γ_c and Id2 (ref. 16), critical for the differentiation of LTi cells, are also required for the development of FALC c-Kit$^+$Sca-1$^+$ cells. However, this population was present in *Rorc*$^{GFP/GFP}$ mice, which lack LTi cells[17]. FALCs were also present in *aly/aly* mice (Supplementary Fig. 4) but *Rorc*$^{GFP/GFP}$ and *aly/aly* mice have reduced percentages of c-Kit$^+$Sca-1$^+$ cells (Fig. 2d). Mutations in SCF (*Sl/Sl*^{d}) and c-Kit (*W/W*^{v}) resulted in the reduction of c-Kit$^+$Sca-1$^+$T1/ST2$^+$ cells (Fig. 2e), suggesting that the SCF/c-Kit pathway is in part involved in the differentiation of FALC c-Kit$^+$Sca-1$^+$ cells.

The gene expression pattern of sorted FALC c-Kit$^+$Sca-1$^+$ cells examined by microarray analysis differed from those of thymic DN2 and LTi cells (Supplementary Fig. 5). *Tnfrsf11a* (encoding RANK) and *Rorc* (encoding RORγ) were expressed in LTi cells but not in FALC c-Kit$^+$Sca-1$^+$ cells (Supplementary Fig. 5). Semi-quantitative PCR with reverse transcription (RT–PCR) analysis supported these differences (Fig. 2f). The lack of RORγ expression also indicates that these cells are distinct from IL22-producing NKp46$^+$ cells, which express a high amount of RORγ[15]. T1/ST2 was highly expressed on FALC c-Kit$^+$Sca-1$^+$ cells (Fig. 2c) but not on DN2 or LTi cells (data not shown). These results collectively indicate that FALC c-Kit$^+$Sca-1$^+$ cells belong to a new lymphocyte lineage characterized by the expression of c-Kit, IL7R and IL33R. FALC c-Kit$^+$Sca-1$^+$ cells expressed several T_H2 cytokines including IL4, IL5, IL6 and IL13 (Fig. 2g). Consistently, the expression of T_H2-related genes such as *Maf* (c-Maf), *Gata3* (Gata3), *Junb* (JunB) and *Stat6* (Stat6) were readily detected in FALC c-Kit$^+$Sca-1$^+$ cells (Fig. 2h).

Among the cytokines tested—including Flt3l, SCF (also known as Kitl), IL1β, IL2, IL3, IL4, IL5, IL6, IL7, IL9, IL15, IL25, IL33, M-CSF (Csf1), GM-CSF (Csf2), TNFα and TGFβ1—we found that SCF and IL7 supported the survival of FALC c-Kit$^+$Sca-1$^+$ cells (Fig. 3a and data not shown), as expected by their expression of c-Kit and IL7Rα. These cells survived for several weeks on TSt-4 feeder cells (Supplementary Fig. 3) and proliferated in response to IL2 for an extended time period (up to 42 days) without changing surface phenotype (Fig. 3a and Supplementary Fig. 6), raising the possibility that these cells are terminally differentiated effector cells. ELISA analyses showed that FALC c-Kit$^+$Sca-1$^+$ cells are indeed capable of producing large amounts of IL2, IL4, IL5, IL6, GM-CSF and a moderate amount of IFNγ in response to phorbol myristate acetate (PMA) plus ionomycin (Fig. 3b). The amounts of T_H2 cytokines produced by FALC c-Kit$^+$Sca-1$^+$ cells (Fig. 3b, filled bars) were substantially higher than those produced by CD4$^+$ T cells from spleen (Fig. 3b, open bars) or mesenteric lymph nodes (MLN) (Fig. 3b, grey bars). IL5 and IL6 were detected even in the culture with IL7 alone, and IL2 increased the production of these cytokines. Concanavalin A and LPS (lipopolysaccharide) had no effect on cytokine production. Notably, IL33 and a combination of IL2 and IL25 induced extremely high amounts of IL5 and IL13 (microgram amounts from 5,000 cells) but little IFNγ (Fig. 3c, d). IL33 did not induce IL17 production. Basophils and mast cells also express T1/ST2 and produce IL13 in response to IL33 (refs 18, 19),

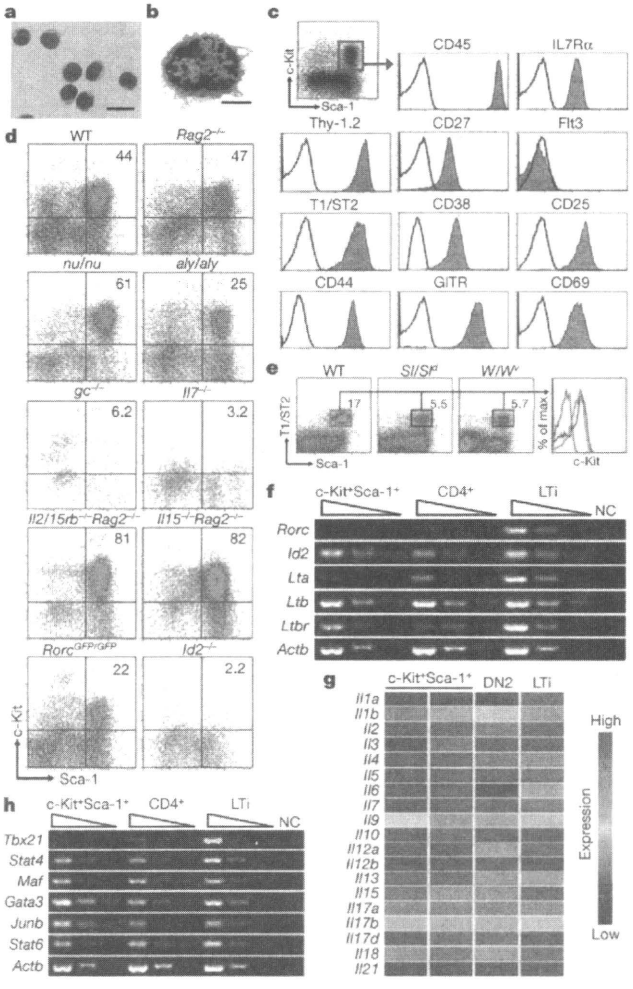

Figure 2 | c-Kit$^+$Sca-1$^+$ cells of FALCs are a new lymphocyte population. **a**, **b**, Giemsa staining (**a**) and electron micrograph (**b**) of sorted FALC c-Kit$^+$Sca-1$^+$ cells. Scale bars, 20 μm (**a**) and 2 μm (**b**). **c**, Flow cytometry of FALC c-Kit$^+$Sca-1$^+$ cells. **d**, **e**, Flow cytometry of mesenteric cells from the indicated strains of mice. Numbers indicate the percentages of c-Kit$^+$Sca-1$^+$ (**d**) and Sca-1$^+$T1/ST2$^+$ (**e**) cells. Histograms in **e** show the expression levels of c-Kit on wild-type (green), *Sl/Sl*^{d} (blue) and *W/W*^{v} (red) Sca-1$^+$T1/ST2$^+$ cells. **f**, **h**, Semi-quantitative RT–PCR analysis of the indicated genes. NC, negative control (no template). **g**, Microarray analysis of cytokine gene expression of FALC c-Kit$^+$Sca-1$^+$ (in duplicate), DN2 and LTi cells.

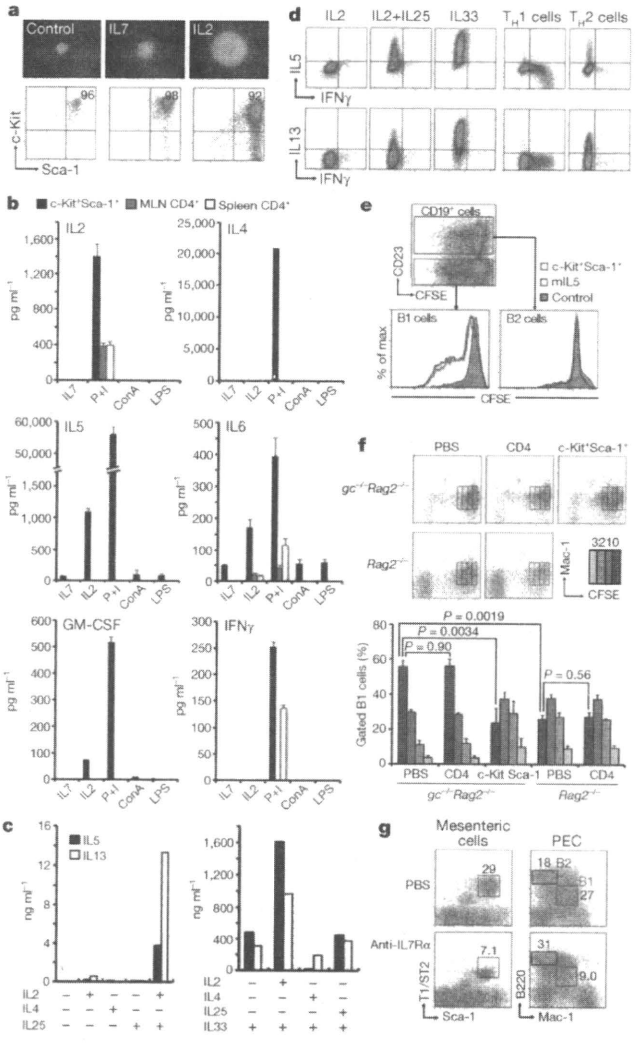

Figure 3 | FALC c-Kit$^+$Sca-1$^+$ cells produce T_H2 cytokines and support B1 cell proliferation. **a**, FALC c-Kit$^+$Sca-1$^+$ cells (5,000 cells per well) were cultured with the indicated cytokines (10 ng ml^{-1}) for 8 days. Bottom panels show flow cytometry of cultured FALC c-Kit$^+$Sca-1$^+$ cells on day 8. **b**, FALC c-Kit$^+$Sca-1$^+$ cells, and CD4$^+$ T cells from MLN or spleen (1×10^4 cells per well) were cultured with the indicated reagents for 3 days, and culture supernatants were analysed in triplicate by ELISA for the indicated cytokines. ConA, concanavalin A; P+I, PMA plus ionomycin. **c**, FALC c-Kit$^+$Sca-1$^+$ cells (5,000 cells per well) were cultured with the indicated cytokines (10 ng ml^{-1}) for 5 days, and culture supernatants were analysed in triplicate by ELISA. **d**, Intracellular cytokine staining of FALC c-Kit$^+$Sca-1$^+$ cells stimulated with the indicated cytokines, and T_H1 and T_H2 cells stimulated with PMA plus ionomycin. **e**, CFSE-labelled B cells (5×10^5) isolated from the peritoneal cavity were cultured with 1.8×10^5 FALC c-Kit$^+$Sca-1$^+$ cells (red line) or 10 ng ml^{-1} IL5 (blue line) as described in Methods. CFSE dilution patterns were examined on CD19$^+$CD23$^-$ B1 cells and CD19$^+$CD23$^+$ B2 cells. **f**, CFSE-labelled B1 cells were transferred intraperitoneally into *Rag2*$^{-/-}$ or *gc*$^{-/-}$ *Rag2*$^{-/-}$ mice (2.5×10^5 per mouse) with the indicated cells. CFSE dilution patterns of B1 cells in recipient mice (three mice per group) were examined on day 9 (top panels). Percentages of cells dividing 0, 1, 2 or 3 times were calculated and the statistics of differences of undivided cells are shown (bottom panel). **g**, Reduction of FALC c-Kit$^+$Sca-1$^+$ cells (left) and peritoneal B1 cells (right) after administration of anti-IL7Rα as described in Methods. PEC, peritoneal exudate cells. All results are representatives of two to three independent experiments. Data in bar charts are shown as the mean and s.e.m.

but the amounts produced were considerably lower (Supplementary Fig. 7).

IL5 is a critical growth factor for B1 cells, which are abundant in the peritoneal cavity and have a crucial role in innate-type immune responses by producing natural antibodies[7]. Peritoneal cavity B cells comprised of both B1 and B2 cells were labelled with carboxyfluorescein succinimidyl ester (CFSE) and cultured with or without FALC c-Kit$^+$Sca-1$^+$ cells. As shown in Fig. 3e, FALC c-Kit$^+$Sca-1$^+$ cells induced the division of CD23$^-$ B1 cells, as did the addition of recombinant IL5, whereas CD23$^+$ B2 cells barely divided. Such B1 cell division was blocked by the addition of anti-mouse IL5 neutralizing antibody (TRFK5) (data not shown). Comparison of cell division of CFSE-labelled B1 cells transferred into *Rag2*$^{-/-}$ mice bearing FALCs or *gc*$^{-/-}$ *Rag2*$^{-/-}$ mice devoid of FALCs demonstrated that B1 cells transferred into *Rag2*$^{-/-}$ mice divided more (Fig. 3f). Co-transfer of FALC c-Kit$^+$Sca-1$^+$ cells but not CD4$^+$ T cells into *gc*$^{-/-}$ *Rag2*$^{-/-}$ mice induced B1 cell division (Fig. 3f). The administration of anti-IL7Rα but not anti-c-Kit monoclonal antibody resulted in the reduction of FALC c-Kit$^+$Sca-1$^+$ cells and peritoneal B1 cells (Fig. 3g and data not shown). These results collectively indicate that FALC c-Kit$^+$Sca-1$^+$ cells support the self-renewal of B1 cells *in vivo*.

IL5 and IL6 regulate B-cell antibody production[5,6]. When FALC c-Kit$^+$Sca-1$^+$ cells were co-cultured with splenic B cells, IgA production was induced (Supplementary Fig. 8), suggesting that FALC c-Kit$^+$Sca-1$^+$ cells have a helper function in IgA secretion. Because there was no increase in the number of surface IgA$^+$ cells after the cultivation of B cells with FALC c-Kit$^+$Sca-1$^+$ cells (data not shown), FALC c-Kit$^+$Sca-1$^+$ cells probably accelerate the secretion of IgA from a small population of IgA$^+$ cells present in the culture rather than inducing class switch recombination.

IL5 and IL13 induced by IL25 or IL33 are also important for the mediation of allergic inflammation and protection against helminth infection[8,9,20]. In particular, IL13 has a critical role in goblet cell hyperplasia, which is crucial for mucin secretion leading to helminth expulsion[8,9]. Although IL25 produced by eosinophils and basophils[21] and IL33 produced by endothelial cells, epithelial cells and adipocytes[22,23] induce IL13, the identity of cells producing IL13 has been obscure[9,21,24]. Administration of IL33 to *Rag2*$^{-/-}$ but not *gc*$^{-/-}$ *Rag2*$^{-/-}$ mice induced the production of IL5 and IL13 and goblet cell hyperplasia (Fig. 4a, b). Because *gc*$^{-/-}$ *Rag2*$^{-/-}$ mice have mast cells and basophils, the above results indicate that FALC c-Kit$^+$Sca-1$^+$ cells are the major cell population producing IL5 and IL13 *in vivo* in response to IL33. After *Nippostrongylus brasiliensis* infection, IL5 and IL13 were readily detected in the sera of wild-type and *Rag2*$^{-/-}$ but not *gc*$^{-/-}$ *Rag2*$^{-/-}$ mice (Fig. 4c). Induction of messenger RNAs for IL5 and IL13 in the mesentery and goblet cell hyperplasia were observed in wild-type and *Rag2*$^{-/-}$ but not *gc*$^{-/-}$ *Rag2*$^{-/-}$ mice (Fig. 4d, e). *N. brasiliensis* infection induced sufficient IL33 in the peritoneal cavity of *Rag2*$^{-/-}$ mice to induce IL13 from FALC c-Kit$^+$Sca-1$^+$ cells (Fig. 4f and Supplementary Fig. 9). Adoptive transfer of FALC c-Kit$^+$Sca-1$^+$ cells into the peritoneal cavity resulted in the production of serum IL13 and goblet cell hyperplasia in helminth-infected *gc*$^{-/-}$ *Rag2*$^{-/-}$ mice (Fig. 4g, h). CD4$^+$ T-cell transfer did not induce serum IL13 until 2 weeks later when 100–300 pg ml^{-1} IL13 was detected in the sera. These results indicate that the contribution of FALC c-Kit$^+$Sca-1$^+$ cells to the production of IL13 and goblet cell hyperplasia after *N. brasiliensis* infection is independent of T cells.

FALC c-Kit$^+$Sca-1$^+$IL7Rα$^+$T1/ST2$^+$ cells proliferate in response to IL2 and produce large amounts of T_H2 cytokines, which support the self-renewal of B1 cells and goblet cell hyperplasia after helminth infection. Such IL2-dependent growth and innate-type effector functions are shared by NK cells, a T_H1 type innate lymphocyte subset. Hence, we propose that FALC c-Kit$^+$Sca-1$^+$IL7Rα$^+$T1/ST2$^+$ cells are T_H2 type innate lymphocytes and that this population therefore be called natural helper cells.

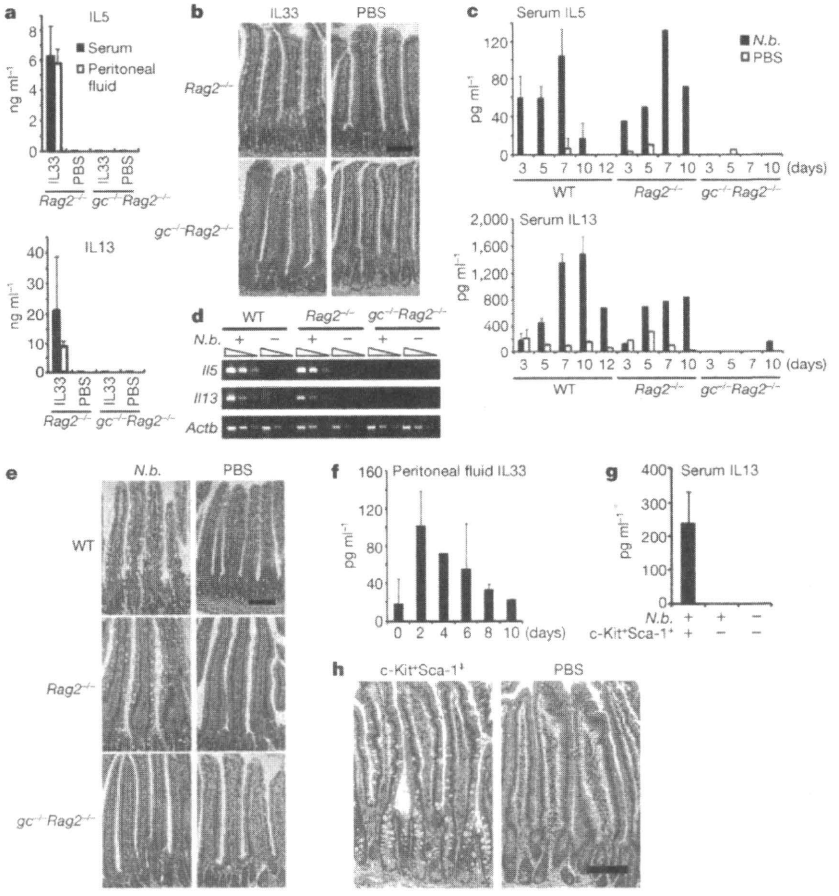

Figure 4 | FALC c-Kit$^+$Sca-1$^+$ cells produce IL5 and IL13 in response to IL33 and induce goblet cell hyperplasia after helminth infection. **a**, **b**, IL33 (0.125 μg in PBS) or PBS alone was administered intraperitoneally to *Rag2*$^{-/-}$ or *gc*$^{-/-}$ *Rag2*$^{-/-}$ mice (two mice per group) every 2 days three times. **a**, Cytokine levels in the serum and peritoneal fluid were determined in triplicate by ELISA on day 7. **b**, Goblet cell hyperplasia in the small intestine was examined on day 7. Goblet cells are seen as white round circles along the surface of villi. **c**–**e**, The indicated strains of mice were infected by subcutaneous injection of 500 *N. brasiliensis* (*N.b.*) larvae. **c**, Serum cytokine levels were analysed in triplicate by ELISA on the indicated days after infection. The numbers of wild-type (WT), *Rag2*$^{-/-}$ and *gc*$^{-/-}$ *Rag2*$^{-/-}$ mice analysed each day were 2, 1 and 1, respectively. Experiments were performed twice and similar results were obtained. **d**, Expression of *Il5* and *Il13* mRNAs by mesentery cells was determined by RT–PCR 14 days after infection. **e**, Goblet cell hyperplasia in the small intestine on day 10 after infection. **f**, Production of IL33 in the peritoneal cavity after *N. brasiliensis* infection. The peritoneal cavity of two mice was washed with 300 μl PBS on each day and assayed for IL33 in triplicate. **g**, **h**, FALC c-Kit$^+$ Sca-1$^+$ cells (2.5 × 10^5) or PBS alone were transferred intraperitoneally into *gc*$^{-/-}$ *Rag2*$^{-/-}$ mice 1 month after *N. brasiliensis* infection (two mice per sample). One week after cell transfer, serum IL13 levels (**g**) and goblet cell hyperplasia in the small intestine (**h**) were examined. All scale bars, 200 μm. Results are representative of two to three independent experiments. Data in bar charts are shown as the mean and s.e.m.

METHODS SUMMARY

Preparation of FALC cells. Mesenteries separated from intestine and mesenteric lymph nodes were cut into small fragments with scissors, and digested in DMEM containing 2 mg ml^{-1} collagenase type I and 4% BSA. The supernatant was aspirated off after centrifugation to remove adipocytes. Finally, cells were suspended in HBSS containing 10% FCS after filtration through a 32-μm nylon mesh.

Full Methods and any associated references are available in the online version of the paper at www.nature.com/nature.

Received 6 October; accepted 5 November 2009.
Published online 20 December 2009.

1. Lodoen, M. B. & Lanier, L. L. Natural killer cells as an initial defence against pathogens. *Curr. Opin. Immunol.* **18**, 391–398 (2006).
2. Andoniou, C. E., Andrews, D. M. & Degli-Esposti, M. A. Natural killer cells in viral infection: more than just killers. *Immunol. Rev.* **214**, 239–250 (2006).
3. Kawamoto, H. & Katsura, Y. A new paradigm for hematopoietic cell lineages: revision of the classical concept of the myeloid-lymphoid dichotomy. *Trends Immunol.* **30**, 193–200 (2009).
4. Nishikawa, S., Honda, K., Vieira, P. & Yoshida, H. Organogenesis of peripheral lymphoid organs. *Immunol. Rev.* **195**, 72–80 (2003).
5. Sonoda, E. *et al.* Transforming growth factor β induces IgA production and acts additively with interleukin 5 for IgA production. *J. Exp. Med.* **170**, 1415–1420 (1989).
6. Beagley, K. W. *et al.* Interleukins and IgA synthesis. Human and murine interleukin 6 induce high rate IgA secretion in IgA-committed B cells. *J. Exp. Med.* **169**, 2133–2148 (1989).
7. Erickson, L. D., Foy, T. M. & Waldschmidt, T. J. Murine B1 B cells require IL-5 for optimal T cell-dependent activation. *J. Immunol.* **166**, 1531–1539 (2001).
8. Knight, P. A., Brown, J. K. & Pemberton, A. D. Innate immune response mechanisms in the intestinal epithelium: potential roles for mast cells and goblet cells in the expulsion of adult *Trichinella spiralis*. *Parasitology* **135**, 655–670 (2008).
9. Fallon, P. G. *et al.* Identification of an interleukin (IL)-25-dependent cell population that provides IL-4, IL-5, and IL-13 at the onset of helminth expulsion. *J. Exp. Med.* **203**, 1105–1116 (2006).
10. Cao, X. *et al.* Defective lymphoid development in mice lacking expression of the common cytokine receptor γ chain. *Immunity* **2**, 223–238 (1995).
11. Tsuji, M. *et al.* Requirement for lymphoid tissue-inducer cells in isolated follicle formation and T cell-independent immunoglobulin A generation in the gut. *Immunity* **29**, 261–271 (2008).
12. Rangel-Moreno, J. *et al.* Omental milky spots develop in the absence of lymphoid tissue-inducer cells and support B and T cell responses to peritoneal antigens. *Immunity* **30**, 731–7343 (2009).
13. Schmitz, J. *et al.* IL-33, an interleukin-1-like cytokine that signals via the IL-1 receptor-related protein ST2 and induces T helper type 2-associated cytokines. *Immunity* **23**, 479–490 (2005).

14. Watanabe, Y. *et al.* A murine thymic stromal cell line which may support the differentiation of $CD4^-8^-$ thymocytes into $CD4^+8^-$ αβ T cell receptor positive T cells. *Cell. Immunol.* **142,** 385–397 (1992).
15. Sanos, S. L. *et al.* RORγt and commensal microflora are required for the differentiation of mucosal interleukin 22-producing $NKp46^+$ cells. *Nature Immunol.* **10,** 83–91 (2009).
16. Yokota, Y. *et al.* Development of peripheral lymphoid organs and natural killer cells depends on the helix–loop–helix inhibitor Id2. *Nature* **397,** 702–706 (1999).
17. Eberl, G. *et al.* An essential function for the nuclear receptor RORγt in the generation of fetal lymphoid tissue inducer cells. *Nature Immunol.* **5,** 64–73 (2004).
18. Arend, W. P., Palmer, G. & Gabay, C. IL-1, IL-18, and IL-33 families of cytokines. *Immunol. Rev.* **223,** 20–38 (2008).
19. Kroeger, K. M., Sullivan, B. M. & Locksley, R. M. IL-18 and IL-33 elicit Th2 cytokines from basophils via a MyD88- and p38α-dependent pathway. *J. Leukoc. Biol.* **86,** 769–778 (2009).
20. Humphreys, N. E., Xu, D., Hepworth, M. R., Liew, F. Y. & Grencis, R. K. IL-33, a potent inducer of adaptive immunity to intestinal nematodes. *J. Immunol.* **180,** 2443–2449 (2008).
21. Wang, Y. H. *et al.* IL-25 augments type 2 immune responses by enhancing the expansion and functions of TSLP-DC-activated Th2 memory cells. *J. Exp. Med.* **204,** 1837–1847 (2007).
22. Haraldsen, G., Balogh, J., Pollheimer, J., Sponheim, J. & Küchler, A. M. Interleukin-33—cytokine of dual function or novel alarmin? *Trends Immunol.* **30,** 227–233 (2009).
23. Wood, I. S., Wang, B. & Trayhurn, P. IL-33, a recently identified interleukin-1 gene family member, is expressed in human adipocytes. *Biochem. Biophys. Res. Commun.* **384,** 105–109b (2009).
24. Voehringer, D., Reese, T. A., Huang, X., Shinkai, K. & Locksley, R. M. Type 2 immunity is controlled by IL-4/IL-13 expression in hematopoietic non-eosinophil cells of the innate immune system. *J. Exp. Med.* **203,** 1435–1446 (2006).

Supplementary Information is linked to the online version of the paper at www.nature.com/nature.

Acknowledgements We thank Y. Yokota and H. Kiyono for *Id2*$^{-/-}$ mice, D. Littman and S. Fagarasan for *Rorc*$^{GFP/GFP}$ mice, T. W. Mak for *Il2/15rb*$^{-/-}$ mice, K. Ikuta for *Il7*$^{-/-}$ mice, and K. Ishiwata for *N. brasiliensis*. Thanks are also owed to L. K. Clayton for critical reading of the manuscript and valuable suggestions, M. Fujiwara for help with microarray analysis, Y. Baba and A. Minowa for help with some experiments, and K. Takei and K. Hidaka for animal care. This work was supported by a Keio University Grant-in-Aid for Encouragement of Young Medical Scientists (to K.M.), a Grant-in Aid for Young Scientist (B) (20790378 to K.M.), Grants-in-Aid for Scientific Research (B) (14370116, 16390146, 18390155 to S.K.) from the Japan Society for the Promotion of Science, and a Scientific Frontier Research Grant from the Ministry of Education, Culture, Sports, Science and Technology, Japan. K.M. is a postdoctoral fellow of the Global COE program supported by the Ministry of Education, Culture, Sports, Science and Technology, Japan.

Author Contributions K.M. conceived the study, performed experimental work, and wrote the paper; T.Y. performed the pathological work; M.T. and T.T. performed the helminth infection experiments; T.I. and H.K. performed the lymphoid progenitor assay; J.-i.F., M.O. and H.F. performed experiments, interpreted data and provided intellectual input; and S.K. conceived the study and wrote the paper.

Author Information Reprints and permissions information is available at www.nature.com/reprints. The authors declare competing financial interests: details accompany the full-text HTML version of the paper at www.nature.com/nature. Correspondence and requests for materials should be addressed to S.K. (koyasu@sc.itc.keio.ac.jp).

METHODS

Mice. Mice used in this study were on a C57BL/6 background unless otherwise stated, and maintained at Taconic or in our animal facility under specific pathogen-free conditions. Wild-type C57BL/6 mice were purchased from Japan SLC. W/W^v mice[25], Sl/Sl^d mice[26] and *aly/aly* mice[27] were obtained from CLEA Japan. W/W^v and Sl/Sl^d mice were on a WBB6F1 background and we used wild-type mice on a WBB6F1 background as control mice. $Rag2^{-/-}$ (stock no. RAGN12)[28], $gc^{-/-}$ $Rag2^{-/-}$ (stock no. 4111)[10,28], $Il15^{-/-}$ (stock no. 4269)[29], and *nu/nu* (stock no. B6NU) mice were purchased from Taconic. $gc^{-/-}$ mice were obtained by mating $gc^{-/-}$ $Rag2^{-/-}$ mice with wild-type C57BL/6 mice. $Il15^{-/-}$ $Rag2^{-/-}$ mice were obtained by crossing $Il15^{-/-}$ and $Rag2^{-/-}$ mice. Inhibitor of DNA binding 2 $(Id2)^{+/-}$ and $Id2^{-/-}$ mice[16] on a mixed genetic background (129/Sv × NMRI) were provided by H. Kiyono. $Rorc^{GFP/GFP}$ mice[17], $Il2/15rb^{-/-}$ (also known as $Il2rb^{-/-}$) mice[30] and $Il7^{-/-}$ mice[31] were provided by S. Fagarasan, T. W. Mak and K. Ikuta, respectively. All experiments were approved by the Animal Care and Use Committee of the Keio University and were performed in accordance with the institutional guidelines.

Human samples. The use of human samples from autopsies was generously permitted by the bereaved families.

Antibodies and reagents. Monoclonal antibodies specific for mouse c-Kit (2B8), Sca-1 (E13-161), CD25 (PC61), CD38 (90), CD44 (IM7), CD69 (H1.2F3), Flt3 (A2F10.1), Thy-1.2 (CD90.2), FcγR (2.4G2), CD3ε (145-2C11), CD4 (GK1.5), CD8α (53-6.7), TCRβ (H57-597), TCRδ (GL3), Gr-1 (RB6-8C5), erythroid cell marker (TER-119), CD19 (1D3), CD11c (HL3), Mac-1 (M1/70), NK1.1 (PK136), CD49b/pan-NK cells (Dx5), CD45 (104), B220 (RA3-6B2), CD40 (HM40-3), CD28 (37.51), IL4 (11B11), IL12 (C17.8), IFNγ (XMG1.2) and anti-human c-Kit monoclonal antibody (104D2) were purchased from BD Pharmingen. Monoclonal antibodies against mouse IL5 (TRFK5), c-Kit (ACK2), IL7Rα (A7R34), CD27 (LG.7F9), GITR (DTA-1), FcεRIα (MAR-1), IL13 (eBio13A) and anti-human IL7Rα monoclonal antibody (eBioRDR5) were purchased from eBioscience. Anti-mouse CD23 (B3B4) and anti-mouse T1/ST2 monoclonal antibodies were purchased from Caltag Laboratories and MD Bioscience, respectively. Allophycocyanin (APC)-conjugated streptavidin was used to reveal staining with biotinylated monoclonal antibodies. Four-colour flow cytometry was performed on a FACSCalibur (BD Bioscience). Cells were gated through a lymphocyte gate defined by FSC and SSC, and dead cells were gated out by propidium iodide.

mIL3, mIL4, mIL5, mIL6, mIL7, mIL9, mIL12, hFlt3l (also known as hFLT3LG), mSCF, mM-CSF, mGM-CSF and hTGFβ1 were purchased from PeproTech, hIL2 from Shionogi Pharmaceutical Co., mBAFF (also known as mTnfsf13b), mIL15, mTNFα, mIL25 and mIL33 were from R&D systems, LPS (*Escherichia coli* 055: B5), concanavalin A and PMA from Sigma, and ionomycin from Calbiochem.

Preparation of cell suspensions. Mice were transcardially perfused with 10 U ml^{-1} heparin in PBS under nembutal anaesthesia. Mesenteric tissues were carefully separated from the intestines, and mesenteric lymph nodes were removed. Samples were cut into small fragments with scissors, transferred to a 15-ml tube in 5 ml of DMEM containing 2 mg ml^{-1} collagenase type I (GIBCO) and 4% BSA (Sigma), then digested at 37 °C by shaking at 1*g* for 45 min. We added 10 μg ml^{-1} DNase I (Roche) for human samples. The supernatant was aspirated off after centrifugation to remove adipocytes. Finally, cells were suspended in HBSS containing 10% FCS after filtration with a 32-μm nylon mesh. To purify Lin$^-$c-Kit$^+$Sca-1$^+$ cells, cells were enriched for Lin$^-$ cells by negative sorting on an AutoMACS (Miltenyi Biotec GmbH) with a combination of magnetic beads conjugated with monoclonal antibodies against CD4, CD8α, CD11c, B220, NK1.1, Mac-1, Gr-1, TER119 and FcεRIα. Subsequently, samples were stained with monoclonal antibodies against other Lin markers (CD3, CD5, CD19, TCRβ, TCRδ), c-Kit and Sca-1, and sorted on a FACSAria (BD Bioscience).

Bone-marrow-derived mast cells and basophils were prepared by culturing bone marrow cells with 20% WEHI-3 culture supernatant for 7 days, stained with monoclonal antibodies against c-Kit, FcεRIα and CD49b followed by sorting c-Kit$^+$FcεRIα$^+$CD49b$^-$ (mast cells) and FcεRIα$^+$CD49b$^+$ cells (basophils). Thymic DN2 cells were prepared from adult thymocytes. Thymocytes were stained with magnetic beads conjugated with anti-CD4 and anti-CD8α monoclonal antibodies and CD4$^-$CD8$^-$ double negative (DN) cells were negatively sorted by AutoMACS. Double-negative cells were further stained with anti-CD25 and anti-CD44 monoclonal antibodies, and CD25$^+$CD44$^+$ cells were sorted as DN2 cells on a FACSAria. Thy-1$^+$CD4$^-$ LTi cells were prepared from fetal liver cells as described previously[32]. c-Kit$^+\alpha_4\beta_7{}^+$IL7Rα$^+$ fetal liver cells from day 13 embryos were cultured on TSt-4 cells for 17 days.

Electron microscopy. Sorted Lin$^-$c-Kit$^+$Sca-1$^+$ cells were centrifuged, and the cell pellets were fixed in 2.5% glutaraldehyde in 0.1 M sodium cacodylate buffer, pH 7.2, for 1 h. After washing, cells were post-fixed in 1% osmium tetroxide for 2 h, stained en bloc with uranyl acetate, dehydrated in a series of graded ethanol solutions, and embedded in an Epon/Araldite mixture. Ultrathin sections were stained with lead citrate and examined under an electron microscope (Nippon Denshi EX-200).

Microarray analysis. Total RNA was extracted from 5 × 10^5 FALC c-Kit$^+$Sca-1$^+$ cells, LTi cells and DN2 cells after direct sorting into a vial containing ISOGEN LS (Nippon Gene). Total RNA was further purified using an RNeasy Micro Kit (QIAGEN) and amplified by a Two-Cycle Target Labelling method (Affymetrix). Microarray processing was done by the Central Research Laboratory, Keio University School of Medicine. The cRNA was hybridized to GeneChip mouse Genome 430 2.0 Array chips (Affymetrix). Hybridized chips were stained, washed and then scanned with a GeneChip Scanner 3000 7G (Affymetrix). Silicon Genetics software GeneSpring (Tomy Digital Biology) was used for data analysis.

Measurement of cytokines. FALC c-Kit$^+$Sca-1$^+$ cells or CD25$^-$CD11c$^-$CD496$^-$CD4$^+$ cells sorted from the spleen and MLN were seeded at 1 × 10^4 cells per well or 5 × 10^3 cells per well into 96-well round bottom tissue culture plates in RPMI-1640 complete medium (RPMI-1640 medium, Sigma) containing 10% FCS, 50 μM 2-mercaptoethanol (GIBCO), 100 U ml^{-1} penicillin and 100 μg ml^{-1} streptomycin (GIBCO), 1× non-essential amino acids (Sigma), 10 mM HEPES (Sigma), and 1 mM sodium pyruvate (GIBCO) with various stimulants including IL7 (10 ng ml^{-1}), IL2 (10 ng ml^{-1}), PMA (30 ng ml^{-1}) plus ionomycin (500 ng ml^{-1}), concanavalin A (10 μg ml^{-1}), or LPS (5 μg ml^{-1}). Supernatants were collected on day 3 or 5. Cytokine levels in culture supernatants were determined in triplicate by ELISA using Quantikine kits (R&D). Immunoglobulin concentrations were measured by Clonotyping System-HRP (SouthernBiotech). T_H1 and T_H2 cells were prepared by stimulating splenic CD4$^+$ cells in anti-CD3ε-coated plates (5 μg ml^{-1} for 5 h) with anti-CD28 (1 μg ml^{-1}) in the presence of a combination of IL12 (10 ng ml^{-1}) and anti-IL4 (10 μg ml^{-1}), or a combination of IL4 (10 ng ml^{-1}), anti-IL12 (10 μg ml^{-1}) and anti-IFNγ (10 μg ml^{-1}), respectively, for 5 days. Intracellular cytokine staining was performed as follows. T_H1 and T_H2 T cells were stimulated for 3 h with PMA (30 ng ml^{-1}) and ionomycin (500 ng ml^{-1}) in the presence of Brefeldin A at the recommended concentrations (eBioscience). FALC c-Kit$^+$Sca-1$^+$ cells were stimulated with IL33 (10 ng ml^{-1}), IL2 (10 ng ml^{-1}) or a combination of IL2 (10 mg ml^{-1}) and IL25 (10 ng ml^{-1}) for 4 days in the absence of Brefeldin A. Cells were fixed and permeabilized with IntraPrep (Beckman Coulter) and then stained intracellularly with FITC-conjugated anti-IFNγ (XMG1.2), phycoerythrin (PE)-conjugated anti-IL5 (TRFK5) and APC-conjugated anti-IL13 (eBio13A).

Immunofluorescence staining. Mesenteric tissues were embedded in OCT compound (Sakura Fine Tec Japan) and quickly frozen in liquid nitrogen. Frozen sections were cut using a cryostat into 9-μm slices, and were immediately fixed in acetone for 10 min, washed with TBS, pretreated with Block-ace (Dainippon Pharmaceutical) for 15 min at 37 °C, incubated with a 0.3% H_2O_2/0.1% NaN_3 solution for 10 min at room temperature, and washed three times. Rat anti-c-Kit (ACK-2) and hamster anti-CD3ε (145-2C11) monoclonal antibodies were diluted in TBS containing 5% goat serum (Nichirei Biosciences), incubated for 2 h at room temperature, and washed three times with TBS. Subsequently, sections were incubated with Histofine Simple Stain Mouse MAX-PO (Rat) (Nichirei Biosciences) for 1 h at room temperature and washed three times with TBS. Sections were incubated with FITC-conjugated anti-HRP and Alexa fluor 568-conjugated anti-hamster IgG for 2 h at room temperature. PE-conjugated anti-B220 monoclonal antibody was used to stain B cells. Samples were then incubated with 1 μg ml^{-1} DAPI (Invitrogen) for 10 min. Finally, slides were mounted in Fluorescence Mounting Medium (DAKO). Images were acquired under a LSM510META confocal microscope (Carl Zeiss) and images edited with Photoshop software (Adobe Systems).

Giemsa staining. Cytospin specimens of sorted FALC c-Kit$^+$Sca-1$^+$ cells were fixed in methanol for 30 s, dried, and stained with 10% Giemsa stain solution (Wako) for 10 min, then flushed with water.

RT–PCR. Total RNA was purified using the RNeasy Plus Mini kit (QIAGEN). RNA was reverse-transcribed with the Ready-to-go T-primed first-strand kit (Amersham). Primer pairs for *Id2, Rorc, Lta, Ltb, Ltbr, Maf, Gata3, Junb, Stat4, Stat6, Tbx21* and *Actb* (Supplementary Table 1) and Taq polymerase (Bioline) were used for PCR. After incubation at 95 °C for 5 min, products were amplified by 35 cycles of 95 °C for 30 s, 55 °C for 30 s, 72 °C for 30 s and then 72 °C for 5 min. In a different set of experiments, primer pairs for *Il5, Il13* and *Actb* (Supplementary Table 1) and Taq polymerase (Takara) were used for PCR. After incubation at 95 °C for 5 min, products were amplified by 35 cycles of 95 °C for 30 s, 58 °C for 30 s, 72 °C for 15 s and then 72 °C for 5 min. Experiments were performed on fivefold dilutions of cDNA and the amount of cDNA was normalized by *Actb*.

CFSE labelling and adoptive transfer of B1 cells. $CD3^-B220^+$ B cells or $CD3^-B220^{lo}$ B1 cells sorted from peritoneal cavity cells were labelled with 2.5 μM CFSE (Invitrogen) at 37 °C for 5 min and washed twice, then co-cultured with BAFF (50 ng ml^{-1}) alone or with BAFF plus 1.8×10^5 FALC c-Kit$^+$Sca-1$^+$ cells or BAFF plus 10 ng ml^{-1} IL5 for 3 days. Cells were then stained with anti-CD19 and anti-CD23 monoclonal antibodies, and cell division patterns as demonstrated by CFSE dilution were examined on $CD19^+CD23^-$ B1 cells and $CD19^+CD23^+$ B2 cells. For *in vivo* proliferation assays, CFSE-labelled B1 cells were transferred into recipient mice with PBS, 2×10^5 $CD4^+$ T cells or FALC c-Kit$^+$Sca-1$^+$ cells. After 9 days, peritoneal cells were collected and stained with anti-B220 and anti-Mac-1, and CFSE dilution of $B220^+$Mac-1$^+$ B1 cells was analysed by flow cytometry. Percentages of cells dividing 0, 1, 2 and 3 times were calculated.

Administration of anti-IL7 receptor antibodies. PBS or anti-IL7Rα monoclonal antibody (1 mg per mouse) in PBS was administered to wild-type mice on days 0 and 2, and FALC c-Kit$^+$Sca-1$^+$ cells and peritoneal B1 cells were analysed on day 5. The results shown in Fig. 3g are representative of three independent experiments with similar results.

Helminth infection. Mice were inoculated subcutaneously with 500 viable third-stage *N. brasiliensis* larvae in 500 μl PBS[33]. Animals were euthanized 3, 5, 7, 10 and 12 days after infection, and serum for ELISA, mesentery cells for RT–PCR, and small intestines for H&E staining collected. Peritoneal fluids were also collected by washing the peritoneal cavity with 700 μl PBS except that 300 μl PBS were used to wash the peritoneal cavity when measuring IL33. For adoptive transfer, 2.5×10^5 FALC c-Kit$^+$Sca-1$^+$ cells cultured with 10 ng ml^{-1} IL2 for 4 days or splenic $CD4^+$ T cells were transferred intravenously into $gc^{-/-}$ $Rag2^{-/-}$ mice that had been infected with *N. brasiliensis* for 33 days. One week after cell transfer, serum for ELISA and small intestines for H&E staining were isolated.

Statistical analysis. Data are shown as the mean and s.e.m. Statistical analysis was performed using the Mann–Whitney *U*-test.

25. Nocka, K. *et al.* Molecular bases of dominant negative and loss of function mutations at the murine *c-kit*/white spotting locus: W^{37}, W^v, W^{41} and *W. EMBO J.* **9**, 1805–1813 (1990).
26. Hayashi, C., Sonoda, T., Nakano, T., Nakayama, H. & Kitamura, Y. Mast-cell precursors in the skin of mouse embryos and their deficiency in embryos of Sl/Sl^d genotype. *Dev. Biol.* **109**, 234–241 (1985).
27. Miyawaki, S. *et al.* A new mutation, *aly*, that induces a generalized lack of lymph nodes accompanied by immunodeficiency in mice. *Eur. J. Immunol.* **24**, 429–434 (1994).
28. Shinkai, Y. *et al.* RAG-2-deficient mice lack mature lymphocytes owing to inability to initiate V(D)J rearrangement. *Cell* **68**, 855–867 (1992).
29. Kennedy, M. K. *et al.* Reversible defects in natural killer and memory CD8 T cell lineages in interleukin 15-deficient mice. *J. Exp. Med.* **191**, 771–780 (2000).
30. Suzuki, H., Duncan, G. S., Takimoto, H. & Mak, T. W. Abnormal development of intestinal intraepithelial lymphocytes and peripheral natural killer cells in mice lacking the IL-2 receptor β chain. *J. Exp. Med.* 185, 499–505 506 (1997).
31. Maki, K. *et al.* Interleukin 7 receptor-deficient mice lack T cells. *Proc. Natl Acad. Sci. USA* **93**, 7172–7177 (1996).
32. Yoshida, H. *et al.* Expression of $\alpha_4\beta_7$ integrin defines a distinct pathway of lymphoid progenitors committed to T cells, fetal intestinal lymphotoxin producer, NK, and dendritic cells. *J. Immunol.* **167**, 2511–2521 (2001).
33. Ishiwata, K. & Watanabe, N. *Nippostrongylus brasiliensis*: reversibility of reduced-energy status associated with the course of expulsion from the small intestine in rats. *Exp. Parasitol.* **117**, 80–86 (2007).

Bordetella evades the host immune system by inducing IL-10 through a type III effector, BopN

Kanna Nagamatsu,[1] Asaomi Kuwae,[1] Tadashi Konaka,[1] Shigenori Nagai,[3,4] Sei Yoshida,[3,4] Masahiro Eguchi,[2] Mineo Watanabe,[2] Hitomi Mimuro,[5] Shigeo Koyasu,[3,4,6] and Akio Abe[1]

[1]Laboratory of Bacterial Infection and [2]Laboratory of Immunoregulation, Graduate School of Infection Control Sciences, Kitasato University, Tokyo 108-8641, Japan
[3]Department of Microbiology and Immunology, Keio University School of Medicine, Tokyo 160-8582, Japan
[4]Core Research for Evolutional Science and Technology, Japan Science and Technology Agency, Chiyoda-ku, Tokyo 102-0075, Japan
[5]Department of Microbiology and Immunology, Institute of Medical Science, University of Tokyo, Tokyo 108-8639, Japan
[6]Research Center for Science Systems, Japan Society for the Promotion of Science, Chiyoda-ku, Tokyo 102-8472, Japan

The inflammatory response is one of several host alert mechanisms that recruit neutrophils from the circulation to the area of infection. We demonstrate that *Bordetella*, a bacterial pathogen, exploits an antiinflammatory cytokine, interleukin-10 (IL-10), to evade the host immune system. We identified a *Bordetella* effector, BopN, that is translocated into the host cell via the type III secretion system, where it induces enhanced production of IL-10. Interestingly, the BopN effector translocates itself into the nucleus and is involved in the down-regulation of mitogen-activated protein kinases. Using pharmacological blockade, we demonstrated that BopN-induced IL-10 production is mediated, at least in part, by its ability to block the extracellular signal-regulated kinase pathway. We also showed that BopN blocks nuclear translocation of nuclear factor κB p65 (NF-κBp65) but, in contrast, promotes nuclear translocation of NF-κBp50. A BopN-deficient strain was unable to induce IL-10 production in mice, resulting in the elimination of bacteria via neutrophil infiltration into the pulmonary alveoli. Furthermore, IL-10–deficient mice effectively eliminated wild-type as well as BopN mutant bacteria. Thus, *Bordetella* exploits BopN as a stealth strategy to shut off the host inflammatory reaction. These results explain the ability of *Bordetella* species to avoid induction of the inflammatory response.

CORRESPONDENCE
Akio Abe:
abe@lisci.kitasato-u.ac.jp

Abbreviations used: BG, Bordet-Gengou; BMDC, BM-derived DC; ERK, extracellular signal-regulated kinase; IκB, inhibitor of NF-κB; JNK, c-Jun N-terminal kinase; LDH, lactate dehydrogenase; MAPK, mitogen-activated protein kinase; m.o.i., multiplicity of infection; qRT-PCR, quantitative real-time PCR; T3SS, type III secretion system; TLR, Toll-like receptor.

Bordetella pertussis is a causative agent of whooping cough (pertussis) in humans (Mattoo and Cherry, 2005). Recent studies suggest that 48.5 million people suffer from pertussis per year, with as many as 295,000 deaths worldwide (Mattoo and Cherry, 2005). Although wide-scale vaccination has been performed in many countries, major concerns exist about pertussis as a reemerging infectious disease (Gzyl et al., 2001; King et al., 2001; He et al., 2003; Raguckas et al., 2007). For this reason, the identification and characterization of new virulence factors as potential protective antigens is critical for the development of more effective and longer-acting vaccines. Possible candidates for such protective antigens include the component proteins of the type III secretion system (T3SS), a protein transport device composed of two distinct portions: (1) a cylindrical basal body that spans the outer and inner membranes of the bacterium and (2) a needle-like structure that protrudes from the bacterial outer membrane and functions as an injector of bacterial proteins (called effectors) into the host cells (Galán and Wolf-Watz, 2006).

Many Gram-negative bacterial pathogens exploit T3SS to deliver effectors into host cells, thereby altering the physiological functions of the infected cells (Finlay and Cossart, 1997). T3SSs are involved in establishing disease processes, and the virulence of pathogens can be

The Rockefeller University Press $30.00
J. Exp. Med. Vol. 206 No. 13 3073-3088
www.jem.org/cgi/doi/10.1084/jem.20090494

The Journal of Experimental Medicine

greatly reduced in T3SS-deficient strains (Abe et al., 1998). Although *B. pertussis* infection is highly specific to humans, *B. bronchiseptica* is a broad host range pathogen that causes kennel cough in dogs, atrophic rhinitis in swine, snuffles in rabbits, and bronchopneumonia in guinea pigs (Goodnow, 1980; Foley et al., 2002). *B. bronchiseptica* is the evolutionary progenitor of *B. pertussis* and *B. parapertussis*, and many virulence factors and effectors delivered by the T3SS are highly conserved among these three strains (Fauconnier et al., 2001). For these reasons, *B. bronchiseptica* has been used as a model of *B. pertussis*. In *Bordetella*, T3SS as well as adherence factors and toxins are positively regulated by a two-component regulatory system composed of BvgA and BvgS (Stibitz et al., 1989). Thus, activation of the BvgA/BvgS system triggers the bacteria to enter the virulent phase. Five type III–secreted proteins—BopB, BopC (also referred to as BteA), BopD, BopN, and Bsp22—have been identified in *Bordetella* (Yuk et al., 2000; Kuwae et al., 2003, 2006; Nogawa et al., 2004; Panina et al., 2005). We have demonstrated that BopB and BopD make a complex and form translocation pores on the host membrane as a conduit of effectors (Kuwae et al., 2003; Nogawa et al., 2004). Bsp22 polymerizes to form a flexible filamentous structure at the tip of the needle structure and associates with the pore component BopD (Medhekar et al., 2009). The size of the outer diameter and the shape of the Bsp22-mediated filament are similar to those of the enteropathogenic *Escherichia coli* EspA sheath–like structure that is thought to facilitate the ability of the bacteria to traverse the mucus layer and the glycocalyx of the intestinal epithelium (Sekiya et al., 2001). The Bsp22-derived filament may have a similar function in establishing the T3SS-dependent persistent colonization of the respiratory tract. Finally, the *Bordetella* BopC/BteA effector can be translocated into the host cells via the T3SS and the BopB/BopD-mediated translocation pore, and induces necrotic cell death in mammalian cell lines (Panina et al., 2005; Kuwae et al., 2006).

In vivo studies using *B. bronchiseptica* have demonstrated that the T3SS plays a role in the persistent bacterial colonization of the lower respiratory tract by modulating host immune responses; *B. bronchiseptica* infection alters DC maturation and enhances the production of the antiinflammatory cytokine IL-10 (Skinner et al., 2004; Skinner et al., 2005; Pilione and Harvill, 2006), thereby inhibiting production of proinflammatory cytokines such as IFN-γ. Furthermore, *B. bronchiseptica* colonization in IL-$10^{-/-}$ mice is significantly reduced compared with that in WT mice (Skinner et al., 2005; Pilione and Harvill, 2006). In contrast, IFN-$\gamma^{-/-}$ mice exhibit defective clearance of *B. bronchiseptica* compared with WT mice (Pilione and Harvill, 2006). These results suggest that *Bordetella* actively enhances the production of the immunosuppressive cytokine IL-10 as a survival strategy, using certain unknown type III effectors.

In this study, we have identified BopN as the effector involved in the up-regulation of IL-10. We report that the IL-10–mediated antiinflammatory response triggered by a bacterial effector is a *Bordetella* strategy used to escape the host immune system.

RESULTS

The BopN effector is involved in the up-regulation of IL-10

To determine whether the *Bordetella* type III effectors are involved in the up-regulation of IL-10, we established an in vitro model of infection based on a DC cell line (DC2.4). This model mimics DCs expressed in the lower respiratory tract and allows detection of IL-10 mRNA; the expression of IL-10 is modulated by *Bordetella* infection in a T3SS-dependent manner.

DC2.4 cells were infected with WT *B. bronchiseptica* or its isogenic derivatives, the BopC mutant (ΔBopC) and the BopN mutant (ΔBopN), for 60 min. The level of IL-10 mRNA was then measured by quantitative real-time PCR (qRT-PCR; Fig. 1 A). A significantly higher level of IL-10 mRNA was produced in cells infected with WT or ΔBopC compared with ΔBopN or a T3SS mutant (ΔT3SS) strain. The up-regulation of IL-10 was restored in cells infected with ΔBopN complemented with a WT *bopN* clone (ΔBopN/pBopN), indicating that BopN, but not BopC, is involved in IL-10 up-regulation. It is assumed that DC2.4 cells have the ability to uptake bacteria and the resulting phagocytosis event triggers various host-cell signaling pathways. To investigate the involvement of phagocytosis in IL-10 up-regulation, we treated DC2.4 cells with cytochalasin D, a fungal metabolite that inhibits phagocytosis (Fig. 1 B). The level of IL-10 mRNA in DC2.4 cells infected with WT or ΔBopN was not affected by treatment with cytochalasin D. Although the level of IL-10 mRNA in DC2.4 cells infected with ΔT3SS appears to be reduced in the presence of cytochalasin D, no significant difference in the induction of IL-10 was found between ΔBopN and ΔT3SS in the presence or absence of cytochalasin D. Similar results were obtained using *Bordetella* infection of BM-derived DCs (BMDCs), and the level of IL-10 mRNA was significantly reduced after infection with ΔBopN as well as ΔT3SS relative to WT (Fig. 1 C). We also determined the amount of IL-10 by ELISA (Fig. 1 D), and IL-10 production was significantly reduced after infection with ΔBopN as well as ΔT3SS relative to WT. Collectively, these results suggest that the IL-10 up-regulation depends on BopN function and is independent of phagocytosis.

BopN is an essential virulence factor

Our in vitro study demonstrated that *Bordetella* BopN activates the expression of the antiinflammatory cytokine IL-10. This suggested that *Bordetella* may establish persistent colonization and exert full virulence by perturbation of the inflammatory response. Therefore, we investigated BopN function in vivo. C57BL/6J mice were infected intranasally with WT or ΔBopN *B. bronchiseptica* (Fig. 2, A and B). Although all mice infected with WT (5×10^6 bacteria) succumbed by day 5 (Fig. 2 A), all mice infected with ΔBopN or ΔT3SS survived, indicating that the BopN effector is an essential virulence factor. Next, we used a lower dose (5×10^5 bacteria) to mimic

persistent colonization by *Bordetella* (Fig. 2 B). Upon infection with WT, the bacterial number in the lung continued to increase for 5 d, and WT bacteria appeared to establish persistent colonization. In contrast, the number of bacteria in the lung did not increase upon infection with either ΔBopN or ΔT3SS and was significantly decreased after 14 d, indicating that BopN is involved in persistent colonization.

Because neutrophils and macrophages are involved in the elimination of bacteria at an early phase of infection, cells from the lungs of mice infected with *Bordetella* were isolated and analyzed by FACS with anti–Gr-1, anti-CD11b, and anti-CD11c antibodies (Fig. 2, C and D). The lungs of mice infected with WT, ΔBopN, and ΔT3SS contained a large number of $Gr\text{-}1^+/CD11b^+$ cells (neutrophils) at 2 d after infection, but the neutrophil number was greatly reduced by 5 and 8 d (Fig. 2 C). In contrast, at 2 d after infection, the total number of $CD11c^-/CD11b^+$ cells (macrophages) in WT-infected lungs was lower than the number of macrophages in lungs infected with ΔBopN or ΔT3SS (Fig. 2 D). By 5 and 8 d after infection, the numbers of macrophages in the lungs were approximately equal regardless of the strain of *Bordetella*. To further investigate the relative neutrophil or macrophage number involved in bacterial elimination, the total numbers of neutrophils (Fig. 2 C) or macrophages (Fig. 2 D) in the lung were normalized by the bacterial number obtained in Fig. 2 B. The relative number of neutrophils or macrophages in the lung was very different between WT versus ΔBopN or ΔT3SS infection (Fig. 2, E and F).

Lung sections were obtained from mice 2 d after infection with *B. bronchiseptica* WT, ΔbopN, and ΔT3SS (5×10^5 bacteria), and stained with hematoxylin and eosin (H&E; Fig. 2 G). Histological analysis showed edema formation and fibrin deposition in the pulmonary alveoli only in mice infected with the WT strain (Fig. S1). Peribronchiolar edema formation (unpublished data) and infiltration of neutrophils and macrophages into the pulmonary alveoli were observed in mice infected with WT, ΔbopN, and ΔT3SS. However, the degree of neutrophil infiltration into the pulmonary alveoli after ΔBopN infection was significantly higher than the infiltration after WT or ΔT3SS infection (WT, 4 ± 2 cells/100 μm²; ΔbopN, 52 ± 8 cells/100 μm²; ΔT3SS, 2 ± 1 cells/100 μm²; and uninfected, 1 ± 1 cells/100 μm²; Fig. 2 G). A small number of neutrophils was observed in the bronchiolus upon WT infection, whereas a large number of aggregated neutrophils was observed in the bronchiolus upon ΔBopN infection. In contrast, mice infected with ΔT3SS had the appearance of uninfected controls with no histological lesions. These results suggest that BopN counteracts the host inflammatory responses by suppressing neutrophil infiltration into the pulmonary alveoli and bronchiolus, even though the total number of neutrophils in the lung was similar between WT and ΔBopN infection (Fig. 2 C).

Bordetella alters the tracheal microenvironment

To determine the mechanism by which BopN contributes to bacterial colonization in the trachea, mice infected with WT or ΔBopN *B. bronchiseptica* were sacrificed 2 d after infection, and tracheal sections were examined by scanning electron microscopy (Fig. 3, A and B). Upon WT *B. bronchiseptica* infection, bacteria were detected in the trachea (Fig. 3 A, arrowheads) but neither cell-surface damage nor areas of damaged cilia were observed. To our surprise, even though *Bordetella* virulence was greatly reduced upon loss of BopN function (Fig. 2), we observed cell-surface disruption, an

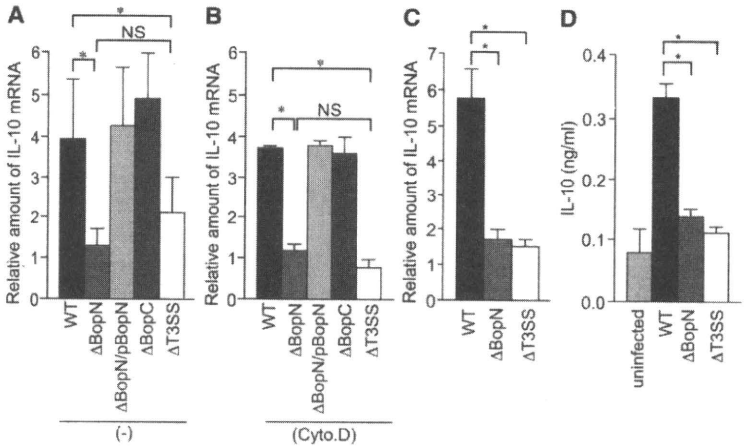

Figure 1. BopN is involved in the up-regulation of IL-10. (A and B) DC2.4 cells were cultured in the absence (A) or presence (B) of 1 μM cytochalasin D (Cyto.D) for 30 min, and then infected with *B. bronchiseptica* WT, BopN effector mutant (ΔBopN), ΔBopN mutant complemented with a WT *bopN* clone (ΔBopN/pBopN), BopC effector mutant (ΔBopC), or T3SS mutant (ΔT3SS). After 60 min, total RNA was prepared and levels of IL-10 mRNA were assessed by real-time PCR using the comparative cycle threshold method. (C) BMDCs were infected with the indicated strains. After 60 min, total RNA was prepared and amounts of IL-10 mRNAs were assessed by real-time PCR. The values in A–C were normalized to the internal control β-actin and calculated in arbitrary units set to a value of 1 for uninfected cells. (D) BMDCs were infected with the indicated strains. After 60 min, the amount of IL-10 in the culture medium was determined by ELISA. The values are means ± SE from three independent experiments. *, $P < 0.05$.